Selective inhibition of NLRP3 inflammasome by designed peptide originating from ASC

Petra Sušjan[1,2], Duško Lainšček[1], Žiga Strmšek[1,2], Vesna Hodnik[3,4], Gregor Anderluh[3] and Iva Hafner-Bratkovič[1,5*]

[1] Department of Synthetic Biology and Immunology, National Institute of Chemistry, Hajdrihova 19, 1000 Ljubljana, Slovenia

[2] Graduate School of Biomedicine, University of Ljubljana, Kongresni trg 12, 1000 Ljubljana, Slovenia

[3] Department of Molecular Biology and Nanobiotechnology, National Institute of Chemistry, Hajdrihova 19, 1000 Ljubljana, Slovenia

[4] Department of Biology, Biotechnical Faculty, University of Ljubljana, Jamnikarjeva 101, Ljubljana, Slovenia

[5] EN-FIST Centre of Excellence, Trg Osvobodilne fronte 13, 1000 Ljubljana, Slovenia

* Corresponding author

E-mail: iva.hafner@ki.si (IH-B)

Telephone: +386 1 4760 393

Short Title: Peptide modulators of NLRP3 inflammasome assembly

ABBREVIATIONS

AAA+ – ATPases associated with various cellular activities; AIM2 – Absent in melanoma 2; ASC – Apoptosis-associated speck-like protein containing a CARD; CAPS – Cryopyrin-associated periodic syndromes; CARD – Caspase activation and recruitment domain; iBMDM – Immortalized bone marrow-derived macrophages; IL-1β – Interleukin-1β; IL-18 – Interleukin-18; LRR – Leucine-rich repeat; NACHT – Domain present in NAIP, CIITA, HET-E, and TP-1; nanoSiO_2 – Nanoparticles of silica; NBD – Nucleotide-binding domain; NLR – Nucleotide-binding domain and leucine-rich repeat containing gene family; NLRC4 – NLR Family CARD Domain Containing 4; NLRP3 – NACHT, LRR and PYD domains-containing protein 3; MRE – Molar residue ellipticity; PYD – Pyrin domain; SEAP – Secreted embryonic alkaline phosphatase; WT – Wild type

ABSTRACT

NLRP3 inflammasome is a multiprotein complex which forms within cells in response to various microbial and self-derived triggers. Mutations in the gene encoding NLRP3 cause rare cryopyrin-associated periodic syndromes (CAPS) and growing evidence links NLRP3 inflammasome to common diseases such as Alzheimer´s disease. In order to modulate different stages of NLRP3 inflammasome assembly nine peptides whose sequences correspond to segments of inflammasome components NLRP3 and ASC were selected. Five peptides inhibited IL-1β release, caspase-1 activation and ASC oligomerization in response to soluble and particulate NLRP3 triggers. Modulatory peptides also attenuated IL-1β maturation induced by constitutive CAPS-associated NLRP3 mutants. Peptide corresponding to H2-H3 segment of ASC pyrin domain selectively inhibited NLRP3 inflammasome by binding to NLRP3 pyrin domain in the micromolar range. The peptide had no effect on AIM2 and NLRC4 inflammasomes as well as NF-κB pathway. The peptide effectively dampened neutrophil infiltration in the silica-induced peritonitis and when equipped with Antennapedia or Angiopep-2 motifs crossed the blood-brain barrier in a mouse model. Our study demonstrates that peptides represent an important tool for targeting multiprotein inflammatory complexes and can serve as the basis for the development of novel anti-inflammatory strategies for neurodegeneration.

Keywords

Inflammation, IL-1β, peptide inhibitors, blood-brain barrier

INTRODUCTION

Inflammasomes are strong proinflammatory complexes needed to fight infection, however they are also prominent drivers of chronic inflammation and can thus importantly contribute to the progression of various diseases including neurodegenerative pathologies. NLRP3 inflammasome complex consists of oligomerized sensor protein NLRP3 (NACHT, LRR and PYD domains-containing protein 3), polymerized adaptor protein ASC (Apoptosis-associated speck-like protein containing a CARD) and molecules of pro-caspase-1, which upon self-activation convert pro-forms of interleukins IL-1β and IL-18 into their active forms and autoinhibited gasdermin D into pore forming N-terminal fragment (1–4). NLRP3 is involved in common diseases such as diabetes (5, 6) and Alzheimer's disease (7, 8) as well as in aging (9). The onset of cryopyrin-associated auto-inflammatory syndromes (CAPS) is associated with the mutations in the NLRP3 gene which render NLRP3 constitutively active (10). NLRP3 inflammasome is primed via NF-κB activation, but needs a second signal, which is provided by a plethora of different agonists such as extracellular ATP and nigericin (11), silica and asbestos particles (12, 13) and amyloid proteins (14, 15). Non-mutated NLRP3 is regarded as the sensor of perturbations in cell homeostasis, particularly as the drop in intracellular K^+ is common to most NLRP3 activators (16–18). Current treatment of CAPS entails antagonizing interleukin-1 signaling using anakinra, rilonacept and canakinumab (19). These drugs block IL-1 signaling, which is mediated by various inflammasomes, and do not inhibit other NLRP3 inflammasome-coupled events such as the release of IL-18 and pyroptosis. Several NLRP3 inflammasome inhibitors including synthetic small molecules MCC950 (20), CY-09 (21), IFN39 (22) and tranilast (23) have been developed. Additionally, natural compounds such as shikonin (24), parthenolide (25) and resveratrol (26) were shown to inhibit NLRP3 inflammasome.

Ordered protein complexes play important functions in immunity (27, 28). NLRP3-mediated ASC polymerization in many ways resembles functional amyloid formation (29). NLRP3 inflammasome assembly is initiated by the oligomerization of NLRP3 molecules via their NACHT domains (30, 31). Pyrin domains (PYD) of oligomerized NLRP3 serve as a docking platform for ASC molecules. Within ASC molecule PYD domain appears to be the main driving force in polymer formation as ASC^{PYD} domain is able to form long filamentous structures (30). CARD (Caspase activation and recruitment domain) domains of ASC on the other hand, recruit pro-caspase-1 into the growing complex and allow crosslinking and condensation of ASC^{PYD} filaments into the ″fur ball″ structures known as specks (32, 33). Consequently, this arrangement of ASC^{CARD} domains tethered on the ASC^{PYD} skeleton provides a multitude of caspase-1 activation sites, which aids significantly in signal amplification (32). ASC specks can be released from cells which further perpetuate proinflammatory response (34, 35). ASC specks were also shown to be able to cross-seed amyloid-β thus increasing Aβ pathology, which could be antagonized using anti-ASC antibody (36). Short peptide fragments

have been used to block amyloid aggregation as reviewed in (37) which encouraged us to use similar principles for the design of modulators of inflammasome assembly.

In this study, we designed a set of putative NLRP3 inflammasome modulatory peptides originating from NLRP3 and ASC in order to inhibit inflammasome complex formation at different stages and different levels of selectivity. We identified a palette of peptides that inhibit the inflammasomes including a peptide originating from ASC^{PYD} domain, that effectively inhibited cytokine release, caspase-1 activation and ASC speck formation in response to various NLRP3 inflammasome activators, while demonstrating no effect on NF-kB pathway or NLRC4 (NLR Family CARD Domain Containing 4) and AIM2 (Absent in melanoma 2) inflammasomes. We showed that this peptide when equipped with peptide internalization tag efficiently penetrates the blood-brain barrier in a mouse model. The peptide efficiently inhibited inflammation in silica-induced peritonitis model.

MATERIALS AND METHODS

Materials

Synthetic peptides were custom synthesized by Proteogenix (Los Angeles, California, US). The following chemicals and kits were used: cell culture media, fetal bovine serum (FBS) and other cell culture supplies (GIBCO, Thermofischer Scientific, Waltham, Massachusetts, US); DMSO, ultra-pure LPS from Escherichia Coli O111:B4, Imject Alum, Phusion HF polymerase (Thermofischer Scientific, Waltham, Massachusetts, US), nanoSiO_2 (nanoparticles of silica), naked poly (dA:dT), QUANTI-Blue, PAM_3CSK_4 (Invivogen, San Diego, CA, US); nigericin, ATP, doxycycline, XTT (Sigma, St. Louis, Missouri, US); mouse IL-1beta Ready-SET-go ELISA (eBioscience, Thermofischer Scientific, Waltham, Massachusetts, US); Lipofectamine 2000 (Thermofischer Scientific, Waltham, Massachusetts, US); FAM-FLICA Caspase-1 Assay Kit (Immunochemistry Technologies, Bloomington, Minneapolis, US); paraformaldehyde (Electron Microscopy Sciences, Philadelphia, Pennsylvania); Histofix (Roth, Karlsruhe, Germany); paraplast, mounting medium CV mount, clear base molds, cassettes (Leica, Wetzlar, Germany); xylene (Fluka, Sigma, St. Louis, Missouri; US); Prolong Diamond Antifade solution with DAPI (Invitrogen, Thermofischer Scientific, Waltham, Massachusetts, US); DOTAP Liposomal Transfection Reagent (Roche, Basel, Switzerland); MCC950 (Avistron Bude, Cornwall, UK); methanol (Merck Darmstadt, Germany); Superdex 200 26/600, NTA sensor chip (GE Healthcare Life Sciences, Chicago, Illinois, US); FAM-FLICA Caspase-1 Assay Kit (Bio-Rad, Hercules, California, US); Retro-X Tet-On 3G inducible expression system (Takara, Clontech, Kusatsu, Shiga Prefecture, Japan). The following antibodies were used: PE anti-ASC (TMS-1) mouse IgG (Biolegend, San Diego, California), Alexa Fluor 488 goat anti-mouse IgG (H+L) (Invitrogen, Thermofischer Scientific, Waltham, Massachusetts, US), anti-Mouse Ly-6G (Gr-1) FITC (eBioscience, Thermofischer Scientific, Waltham,

Massachusetts, US), Caspase-1 p20, Casper-1 (Adipogen, Liestal, Switzerland), HRP-conjugated Goat Anti-Mouse IgG (H+L) polyclonals (Jackson ImmunoResearch, West Grove, Pennsylvania, US), rabbit polyclonal anti-mouse IL1beta (GeneTEX, Irvine, California, United States), goat polyclonal to rabbit IgG (HRP) (Abcam, Cambridge, United Kingdom) and β-Actin (8H10D10) Anti-Mouse mAb (Cell Signaling technology, Danvers, Massachusetts, US).

Cell Cultures

We used immortalized bone marrow derived macrophages (iBMDMs) (13) and immortalized microglia (15) from C57BL/6 mice (a kind gift from Kate A. Fitzgerald and Douglas Golenbock, University of Massachusetts Medical school, Worcester, MA, USA) as well as RAWBlue cells (Invivogen, San Diego, CA, US). Using Retro-X Tet-On 3G inducible expression system (Takara, Clontech) we constructed $NLRP3^{R258W}$ and $NLRP3^{T346M}$ mutants in $NLRP3^{-/-}$ iBMDM as previously described (38). All cell lines were cultured and seeded in DMEM medium supplemented with 10 % FBS. All experiments were performed in serum-free DMEM or OptiMEM.

Peptide Preparation

Lyophilized peptides were dissolved in dimethyl sulphoxide (DMSO) in stock concentration of 10 mM. Prior to use peptides were diluted to the working concentration in serum-free DMEM. As DMSO was shown to inhibit inflammasome activation (39), DMSO concentration (v/v) corresponding to DMSO concentration in peptide preparations was used as control.

Inflammasome and NF-κB Pathway Stimulation

For experiments involving inflammasome stimulation iBMDMs and immortalized microglia cells were seeded in DMEM with 10% FBS at 1.6×10^5 per well of 96-well plate (ELISA, XTT assays), at 0.8×10^6 cells per well of 24-well plate (FAM-FLICA assay), at 1.6×10^6 per well of 6-well plate (Western blotting) and at 2.8×10^5 cells per well of IBIDI slides (immunofluorescence). The next day cells were primed for 6 h with ultra-pure liposaccharide (LPS) (100 ng/mL) or overnight with PAM_3CSK_4 (200 or 500 ng/mL). Medium was removed, cells were washed with phosphate-buffered saline (PBS) and treated with peptides in DMEM for 30 min. Subsequently, different inflammasome instigators in DMEM were added for 1 h (5-10 µM nigericin, 5 mM ATP), 12 h (1 µg/mL poly (dA:dT)/Lipofectamin, 300 µg/mL alum), 4 h (180-200 ng/mL $nanoSiO_2$, 1000 µg/mL WT Saty flagellin/DOTAP). DOTAP and lipofectamin were used according to manufacturer´s instructions. Saty flagellin was produced and used for stimulation as previously described (40). For control

samples, macrophages were treated with medium alone or containing the relevant carrier: DMSO for peptides, DOTAP and lipofectamine for instigators.

For experiments involving NF-κB pathway stimulation RAWBlue cells were seeded in DMEM with 10% FBS at 2.2 x 10^5 cells per well of 96-well plate and left to attach. They were incubated with peptides in DMEM for 30 min. Subsequently, NF-κB activating agents LPS (50 ng/mL) or PAM_3CSK_4 (100 ng/mL) in serum-free DMEM were added for an overnight incubation. Afterwards, secreted embryonic alkaline phosphatase (SEAP) levels in the collected cell supernatants were determined using the QUANTI-Blue assay and recorded as absorbance at 630 nm (A_{630}) using Sinergy Mx (Biotek, Winooski, Vermont, USA).

For experiments involving doxycycline-induced NLRP3 expression in the Retro-X Tet-On 3G inducible expression system (Takara, Kusatsu, Shiga Prefecture, Japan) cells were seeded in DMEM with 10% FBS at 1.2 x 10^5 cells per well of 96-well plate and left overnight. They were incubated with peptides in DMEM for 30 min. Afterwards, NLRP3 expression and inflammasome priming were stimulated with a combination of 100 ng/mL LPS and 1 μg/ml doxycycline (DOX) for 9 h. Afterwards, supernatants were collected and analyzed for IL-1β in ELISA assay.

Cytokine Detection using ELISA Assays

Following cell treatment and stimulation detection of IL-1β in cell supernatants was performed using mouse IL-1beta Ready-SET-go ELISA (eBioscience) according to manufacturer's instructions. Multiplate reader SinergyMx (BioTek, Winooski, Vermont, USA) was used to measure absorbance.

Protein Detection using Western Blotting

Cell stimulation was performed in 6-well plate format. For caspase-1 and IL-1β detection supernatant was concentrated using 3K Amicon Ultra-0.5 mL Centrifugal Filters (Merck Darmstadt, Germany) and centrifugation at 14,000 x g and 4ºC. Concentrate was mixed with SDS and β-mercaptoethanol loading buffer and denatured at 90ºC for 10 min. For pro-caspase-1 and proIL-1β detection cells were washed twice with cold PBS and lysed. Protein concentration in the cell lysate was measured with BCA and mixed with SDS and β-mercaptoethanol loading buffer. Proteins (30 μg per well) were separated on 12% or 15% SDS-PAGE gels, blotted onto the nitrocellulose membrane (GE Healthcare) and detected using iBIND Automated Western System (Thermofisher Scientific, Waltham, Massachusetts, US) with appropriate primary and secondary antibodies. For caspase-1 and pro-caspase-1 detection Caspase-1 p20, Casper-1 (1:1000, Adipogen, Liestal, Switzerland) was used followed by HRP-conjugated Goat Anti-Mouse IgG (H+L) polyclonals (1:600, Jackson

ImmunoResearch, West Grove, Pennsylvania, US). IL-1β and pro-IL-1β were detected using rabbit polyclonal anti-mouse IL1beta (1:1000, GeneTEX, Irvine, California, United States) as primary antibody and goat polyclonal to rabbit IgG (HRP) (1:600, Abcam, Cambridge, United Kingdom) as secondary antibody. As a loading control reference in the case of lysates we used either β-Actin (8H10D10) Anti-Mouse mAb (1:1000, Cell Signaling technology, Danvers, Massachusetts, US) followed by HRP-conjugated Goat Anti-Mouse IgG (H+L) polyclonals (1:600, Jackson ImmunoResearch, West Grove, Pennsylvania, US) or nonspecific band. SuperSignal West Femto or Pico Chemiluminescent Substrate (Thermo Scientific) was used for detection of HRP-labeled bands.

Viability Evaluation using XTT Assay

Cell stimulation and treatment was performed as described. Cell supernatants were removed whereas cells underwent XTT test to determine their viability. For XTT assay, cells were incubated in DMEM without phenol red. A solution of 2,3-bis(2-methoxy-4-nitro-5-sulfophenyl)-5-[(phenylamino)carbonyl]-innersalt-2H-tetrazolium (XTT) and phenazine methosulphate (PMS) in DMEM without phenol red was added to the cells. After 2 and 4 h, absorbance at 490 nm was measured using multiplate reader SinergyMx (BioTek, Winooski, Vermont, USA).

Confocal microscopy

Endogenous ASC was immunofluorescently labeled in fixed and permeabilized WT iBMDMs as previously described (35). Briefly, upon stimulation cells were fixed for 15 min with 4 % PFA without aspiration, washed in PBS and permeabilized and blocked with a mixture of 0.2 % saponin and 1% bovine serum albumin for 1h. After 1h incubation with the ASC-specific primary antibody anti-ASC (TMS-1) mouse IgG (Biolegend, San Diego, California), cells were washed with PBS and incubated for another hour with secondary antibody Alexa Fluor 488 goat anti-mouse IgG (H+L) (Invitrogen, ThermoFisher Scientific, Waltham, Massachusetts, US). Afterwards we added the mounting medium containing nuclei stain Prolong Gold Antifade Mountant with DAPI (ThermoFisher Scientific). Similarly, Angiopep2-ASC$^{PYD/H2\text{-}H3}$-TMR peptide was detected after pretreatment of immortalized microglia cells and subsequent fixation, permeabilization and DAPI staining. For imaging a Leica TCS SP5 laser scanning microscope mounted on a Leica DMI 6000 CS inverted microscope (Leica Microsystems, Wetzlar, Germany) with the HCX plan apo 63× (numerical aperture 1.4) oil immersion objective was used. A 405 nm laser line of 20 mW diode laser was used for DAPI excitation and emitted light was detected between 415 and 450 nm. A 488 nm laser line of 100 mW argon laser with 10 % laser power was used for detection of Alexa 488 conjugate, where emitted light was detected between 500 and 600 nm. A 1 mW 543-nm HeNe laser was used for TMR excitation with emitted light detected between 558-598 nm. For

acquisition and image processing Leica LAS AF and ImageJ software were used. In the case of ASC speck visualization, we recorded images as Z-stacks. Maximal intensity images were then produced to enable detection of all specks within a specific frame. Images were also adjusted for brightness and contrast using Leica LAS AF.

Caspase-1 Detection using Flow Cytometry

Activation of caspase-1 was measured by flow cytometry using a fluorochrome-labeled peptide inhibitor of caspase-1 FAM-YVAD-FMK according to the instructions of FAM-FLICA Caspase-1 Assay Kit manufacturer (Bio-Rad). Briefly, cells were seeded in a 24-well plate and treated with potential peptide inhibitors for 30 min. Afterwards, they were stimulated with a combination of ultra-pure LPS (500 ng/mL) and nigericin (5 µM) for 2,5 h. Fluorescent caspase-1 inhibitor probe FAM-YVAD-FMK was added to wells without aspiration for 30 min. Cells were washed twice on ice, detached in PBS and analyzed by flow cytometer Cyflow (Partec, Munich, Germany) and FloMax or FloJo software.

Protein Interaction Analysis using Surface Plasmon Resonance (SPR)

For the SPR measurement mouse $NLRP3^{PYD}$ encoding sequence with the N-terminal His-tag was prepared with PCR using Phusion HF polymerase and inserted into pRSET A at *BamHI*/*EcoRI* restriction sites. It was transformed into the NiCo2 (DE3) production strain. The production was induced by 1 mM IPTG for 4 h at 37°C. The proteins were then harvested through the centrifugation and lysis of bacterial pellet and subsequent lysate sonication. Upon centrifugation the soluble fraction was purified using the NiNTA resin and eluted in buffer with increasing concentrations of imidazole. The monomeric form of the protein was isolated using size exclusion chromatography (SEC; Superdex 200 26/600, GE Healthcare Life Sciences), concentrated and analyzed with SDS Page electrophoresis and circular dichroism (CD, Applied Photophysics Limited, Leatherhead, Surrey, UK). SPR was performed utilizing the Biacore X100 instrumentation and the NTA sensor chip (both from GE Healthcare Life Sciences, Chicago, Illinois, US). Briefly, upon chip surface activation according to the manufacturer´s instructions, 0.25 nmol of ligand ($NLRP3^{PYD}$-Histag in running buffer 10mM HEPES, 300 mM NaCl, 0.005% Tween 20, pH=8.1) was immobilized onto the test flow cell of the chip, while the reference flow cell was used as a control for nonspecific binding. Then increasing concentrations of the analyte (Angiopep2-$ASC^{PYD/H2-H3}$ in deionized water) were injected into both flow cells at a flow rate of 10 µL/min for 4 min. Between the analyte injections the following chip surface regeneration treatment was used: 350 nM EDTA (1 min), 100 mM NaOH (1 min) and 0.25% SDS (1 min). The specific binding to the ligand was recorded in response units as the difference in signal between ligand-immobilized and reference flow cell.

Animal experiments

Animal experiments were performed according to EU Directive 2010/63 with the permit from the Administration of the Republic of Slovenia for Food Safety, Veterinary and Plant Protection (permit no. U34401-4/2017/4). We used healthy 8 to 12-week-old male and female C57BL/6 mice weighing around 25 grams with normal immune status in all experiments. Mice were housed in the SFP animal facility in an IVC system, fed standard chow and had access to fresh tap water *ad libitum*.

3-5 animals were selected for each treatment group without using any particular randomization method or power calculations for the choice of group size. For the silica-induced murine peritonitis experiment mice were intraperitoneally (i.p.) injected with 30 μmol/kg of $ASC^{PYD/H2-H3}$ peptide or DMSO for 1h using a 29 G needle (Beckton Dickinson). Afterwards 0.35 mg of nanoSiO_2 was injected i.p. in 500uL of PBS for 4 h. Mice were humanely sacrificed with CO_2 asphyxiation followed by the collection of peritoneal lavage. Intraperitoneal cells were isolated through first centrifuging the lavage (10 min centrifugation at 1500 rpm) and pellet resuspension in FACS buffer. Pellet was partly labeled with anti-mouse Ly-6G (Gr-1) FITC antibody for 15 min on ice and partly left unstained. Upon centrifugation the pellet was rinsed with FACS buffer and then fixed in 0.5 mL Histofix (Roth) for 20 min. Upon centrifugation it was washed, rinsed in FACS buffer and left overnight at 4^{o} C before performing cytometry (Partec, Munich, Germany).

To assess transfer through the blood-brain barrier mice were intravenously injected with 0.3 μmol/mouse of peptides Angiopep2-$ASC^{PYD/H2-H3}$-TMR, Antennapedia-$ASC^{PYD/H2-H3}$-TMR, $ASC^{PYD/H2-H3}$-TMR or DMSO in PBS and sacrificed after 1h or 3h. The TMR (tetramethylrhodamine) fluorescence was *in vivo* imaged by using IVIS® Lumina Series III (Perkin Elmer, Waltham, Massachusetts, US). Data were analyzed with Living Image® 4.5.2 (Perkin Elmer, Waltham, Massachusetts, US). Internal organs were then collected and fixed in formalin for histological assessment. Tissue slices were dehydrated by 1h incubation in solutions with increasing ethanol content (1x70%, 1x95%, 3x100%) followed by 1h incubation with xylene (2x) and liquid paraplast (1x). Slices were then placed into the paraplast-filled plastic clear base molds, captured with a cassette and allowed to solidify. Fine tissue slices were cut from the tissue blocks on the microtome (Leica, Wetzlar, Germany) and placed onto glass slides. Paraplast was removed by brief incubation in xylene followed by the tissue slice mounting on the glass slide by mounting medium. Slides were analysed using confocal microscope as described above (Leica Microsystems, Wetzlar, Germany) with HCX PL Fluotar L 20× (numerical aperture 0.4) water objective. A 1 mW 543-nm HeNe laser was used for TMR excitation with emitted light detected at between 558-598 nm. For acquisition and image processing Leica LAS AF and ImageJ software were used.

Statistical Analysis

Unpaired two-tailed t-test with Welch's correction for comparison of populations of different variance was used to compare the groups treated with peptide and solvent in the animal experiment.

RESULTS

Design of putative peptide modulators of inflammasome assembly

The aim of this study was to select peptides that would disrupt intermolecular interactions governing inflammasome assembly at different stages, at NLRP3 oligomerization stage and by disrupting homotypic interactions between PYD domains of NLRP3 and ASC and between CARD domains of ASC and pro-caspase-1 (41) (Fig. 1a). A significant structural information regarding homotypic death domain interactions has been gathered over the past several years (42, 43). PYD and CARD domains consist of a bundle of six α-helices, a motif known as the death fold. Both PYD and CARD domains exhibit extensive oppositely charged patches which regulate homotypic interactions (30, 41). To disrupt PYD-PYD and CARD-CARD interactions between NLRP3, ASC and pro-caspase-1, peptide sequences from PYD and CARD interaction domains of NLRP3 and ASC proteins were selected based on the available structural information (Fig. S1).

The peptide $NLRP3^{PYD/H2\text{-}H3}$ was designed based on the published crystal structure of human $NLRP3^{PYD}$ domain (44) where PYD is present as a dimer with H2-H3 at the homodimeric interface (Fig. S1a). Mutation of several charged residues in this region abolished NLRP3 interaction with ASC (30)ASC is a bipartite adaptor containing non-interacting PYD and CARD domains fused with a long linker (41) (Fig. S1b). ASC^{PYD} has prion-like polymerization properties (45) and forms filamentous structures *in vitro* and when overexpressed in cells (30) (Fig. S1c). H2-H3 segment was selected as it participates in all three types of interface in filament (30, 46). The structure of $NLRP3^{PYD}$ resembles ASC^{PYD} in filament, thus $NLRP3^{PYD}$ might be similarly incorporated into a filament, and $ASC^{PYD/H2\text{-}H3}$ peptide might serve as a disruptor of PYD-PYD interactions between NLRP3 and ASC. Amino acid sequence alignments of PYD domains with marked peptide sequences are presented in Fig. S2a. ASC^{CARD} domain serves for recruitment of pro-caspase-1 but also for crosslinking of ASC^{PYD} filaments (32, 33). Isolated ASC^{CARD} forms filaments (47). Again, we selected the H2-H3 segment as it participates in two out of three types of interactions in ASC^{CARD} filament, and previous studies showed that mutations in specific residues from this segment interfere with pro-caspase-1 recruitment (48) and ASC speck formation (32) (Fig. S1d). Amino acid sequence alignments of CARD domains with depicted selected segments are provided in Fig. S2b.

In the initial stage of inflammasome assembly NLR receptors oligomerize (49–51) through their NACHT domain which comprises nucleotide binding domain and associated domains. A possible site of intervention might also be the blocking of NLRP3 oligomerization. Interestingly, the majority of mutations in the gene encoding NLRP3 currently annotated in Infevers repository (52) are located in this domain (Fig. S3). We observed that some mutations cluster to the areas of $NLRP3^{NACHT}$ that either contain or flank nucleotide binding motifs (53). Peptide segments from ATP binding motifs $NLRP3^{WalkerA}$, $NLRP3^{WalkerB}$ and $NLRP3^{Sens1}$ and additional segments where CAPS associated mutations are clustered were selected. Nomenclature for these NACHT-derived peptides is based on their amino acid position: $NLRP3^{(250-265)}$, $NLRP3^{(427-447)}$ and $NLRP3^{(560-593)}$ (Fig. S3). Selected NACHT segments are depicted in the models and structure of NLRP3 (31) (Fig. S4a-d). Selected peptide segments were equipped with the myristoylation group (54) and accompanying spacer sequence WGG on their N-terminus in order to allow transfer through cell membrane (Fig. S5).

Selected peptides inhibit IL-1β maturation upon canonical NLRP3 inflammasome activation

Upon the design of putative NLRP3 modulators that could act on different protein interactions (Fig. 1a) we characterized their effects on various levels of NLRP3 inflammasome assembly cascade. The first stage in our characterization pipeline was the identification of peptides that exhibited effects on the IL-1β cytokine maturation as the process occurring downstream of inflammasome assembly. For this purpose we primed immortalized bone-marrow derived macrophages (iBMDMs) with LPS, treated them with the peptides and stimulated with particulate NLRP3 inflammasome trigger silica ($nanoSiO_2$). In contrast to the control cells, stimulated in the absence of the peptides, iBMDMs treated with PYD and CARD derived peptides $ASC^{CARD/H2-H3}$, $NLRP3^{PYD/H2-H3}$ and $ASC^{PYD/H2-H3}$ demonstrated a concentration-dependent inhibition of IL-1β release in response to silica (Fig. 1b), while DMSO had no effect (Fig. 1b). Amongst $NLRP3^{NACHT}$ derived peptides, $NLRP3^{WalkerB}$ and $NLRP3^{Sens1}$ inhibited IL-1β secretion in response to silica while no effect was observed with $NLRP3^{WalkerA}$ or the peptides originating from other selected NLRP3 segments ($NLRP3^{(250-265)}$, $NLRP3^{(427-447)}$ and $NLRP3^{(560-593)}$) (Fig. 1b). NLRP3 inflammasome can be activated with a variety of chemically and morphologically distinct triggers. We found that the peptides that attenuated activation of IL-1β with particulate trigger silica ($ASC^{CARD/H2-H3}$, $NLRP3^{PYD/H2-H3}$ and $ASC^{PYD/H2-H3}$, $NLRP3^{WalkerB}$ and $NLRP3^{Sens1}$) also inhibited activation with soluble trigger ATP (Fig. 2a). Inhibitory effects were peptide-related, as the DMSO alone did not inhibit IL-1β release and were not due to potential peptide toxicity as peptides have not affected metabolic activity of treated cells (Fig. 2b). In our screening for potential inflammasome modulating peptides we thus identified five inflammasome modulating peptides originating from $NLRP3^{NACHT}$, $NLRP3^{PYD}$ and ASC^{CARD} domains ($ASC^{CARD/H2-H3}$, $NLRP3^{PYD/H2-H3}$ and $ASC^{PYD/H2-H3}$, $NLRP3^{WalkerB}$ and $NLRP3^{Sens1}$) that effectively

inhibited cytokine release in a concentration-dependent manner in response to different NLRP3 inflammasome triggers.

Peptides attenuate constitutive CAPS-associated activation

Apart from various exogenous triggers, NLRP3 inflammasome activation can also originate from point mutations within the $NLRP3^{NACHT}$ domain that render NLRP3 sensor protein constitutively active. Carrying the mutated NLRP3 variant manifests itself in a set of autoinflammatory diseases. To test whether the peptides would mediate IL-1β inhibition under such circumstances we established an *in vitro* CAPS model where NLRP3-deficient mouse macrophages are reconstituted with doxycycline dependent expression of CAPS-associated mutants: $NLRP3^{R258W}$ or $NLRP3^{T346M}$ (38). Those macrophages were incubated with representative peptides originating from PYD domains ($NLRP3^{PYD/H2\text{-}H3}$ and $ASC^{PYD/H2\text{-}H3}$) and from NACHT domains ($NLRP3^{WalkerB}$) before the induction of NLRP3 expression with doxycycline. All were found to effectively inhibit IL-1β secretion propagated by two constitutively active NLRP3 mutants (Fig. 2c) which extends the inhibitory potential of peptides also to the constitutive NLRP3 inflammasome activation.

Peptides attenuate caspase-1 activation and ASC oligomerization

We were curious whether the peptides inhibiting cytokine release also dampen the activation of caspase-1 responsible for cytokine maturation. Using FAM-YVAD-FMK fluorescent probe which binds active caspase-1 and flow cytometry we labeled active caspase-1 within iBMDMs that have been pretreated with inhibitory peptides $ASC^{CARD/H2\text{-}H3}$, $NLRP3^{PYD/H2\text{-}H3}$ and $ASC^{PYD/H2\text{-}H3}$, $NLRP3^{WalkerB}$ and $NLRP3^{Sens1}$ prior to nigericin-mediated NLRP3 inflammasome activation. We observed significant decrease in active caspase-1 levels within cells treated with all inhibitory peptides in comparison to non-treated and DMSO-treated controls (Fig. 3a). Caspase-1 processing in the presence of selected peptide inhibitors was evaluated also by detecting the p20 subunit of caspase-1. Western blots show reduced levels of caspase-1 subunit p20 when cells were treated with peptides $ASC^{PYD/H2\text{-}H3}$ and $NLRP3^{Sens1}$ in comparison to cells without peptide treatment (Fig. S6a). Pro-caspase-1 levels in the lysate were not affected by the peptide treatment (Fig. S6a). Given the inhibitory role of peptides on the activation of caspase-1 we also addressed the effect of the peptides on the pyroptosis, however the end-point LDH release appeared to be unaffected (data not shown) suggesting that gasdermin D activated through the residual caspase-1 activity is sufficient to enable pyroptosis.

After NLRP3 oligomerization, ASC forms a characteristic speck in the perinuclear region. Using immunolabeling of endogenous ASC we observed that all inhibitory peptides inhibited ASC speck formation in response to nanoSiO_2 as opposed to non-peptide-treated control **(**Fig. 3b,c**)**. Inhibitory effects of NACHT and

PYD derived peptides were expected as they presumably inhibit processes upstream of the ASC oligomerization which is preferentially an ASC^{PYD}-driven process. The fact that ASC^{CARD}-derived peptide ($ASC^{CARD/H2-H3}$) also inhibited ASC speck formation is consistent with recent findings which suggest that the CARD domain is crucial not only for recruitment of pro-caspase-1 but also for speck condensation and nucleation (32). Within this experiment we also tested the peptides that showed no modulatory effect on IL-1β secretion and showed that ASC speck formation was not affected (Fig. S6b,c).

The effect of peptides on the priming step of NLRP3 inflammasome activation

Having identified $NLRP3^{PYD/H2-H3}$, $ASC^{PYD/H2-H3}$ and $ASC^{CARD/H2-H3}$, $NLRP3^{WalkerB}$ and $NLRP3^{Sens1}$ as inflammasome modulators inhibiting cytokine release, caspase-1 activation and ASC oligomerization, we further investigated whether they exhibit any effect on the NLRP3-inflammasome proximate pathways such as the NF-κB pathway involved in the priming step of the NLRP3 inflammasome activation. Several inflammasome inhibitors were also shown to inhibit NF-κB pathway (24). By performing the peptide treatment of iBMDMs after the priming step, our experimental setting ensured that any observed peptide-mediated modulatory effects during the peptide characterization were not an immediate consequence of NF-κB pathway (priming) modulation but rather stemmed from the disruption of inflammasome assembly cascade. To evaluate the extent of modulation that our inhibitory peptides exhibit on the NF-κB pathway we used RawBlue macrophages which encode secreted alkaline phosphatase (SEAP) under the NF-κB/AP-1 promotor. We first performed peptide treatment and then stimulated the cells with LPS. We found that $NLRP3^{WalkerB}$, $ASC^{CARD/H2-H3}$, $NLRP3^{Sens1}$ and $NLRP3^{PYD/H2-H3}$ decreased NF-κB response with $NLRP3^{WalkerB}$ decreasing it strongly and others only at the highest used concentration (Fig. 4a). Among other peptides tested, particularly $ASC^{PYD/H2-H3}$ which inhibited IL-1β maturation, caspase-1 activation and ASC speck formation and inactive peptides $NLRP3^{WalkerA}$, $NLRP3^{(250-265)}$, $NLRP3^{(427-447)}$ did not affect NF-κB pathway (Fig. 4a, Fig. S7a).

The effect on the priming stage (LPS activation) could result from direct neutralization of LPS (55). Indeed, the effect of peptides on NF-κB stimulation by PAM_3CSK_4 was more moderate, only observed at highest concentrations in case of $ASC^{CARD/H2-H3}$ and $NLRP3^{WalkerB}$ (Fig. S7b). However, the peptides retained their inhibitory effect on the IL-1β release when PAM_3CSK_4 was used for inflammasome priming (Fig. S7c). Since ELISA kit used in this study does not distinguish between IL-1β and pro-IL-1β we assessed the pro-IL-1β processing to its bioactive form in the presence of $ASC^{PYD/H2-H3}$ and $NLRP3^{Sens1}$on the protein level (Fig. S7d). While reduced IL-1β levels can be found in the supernatant of cells treated with the peptides, pro-IL-1β levels in the lysate were not affected by the peptide treatment (Fig. S7d). This shows that peptides are indeed inhibiting the processing of the IL-1β rather than having an inhibitory effect on the pro-IL-1β production. Taken

together, these findings suggest that the major effect of peptides is in fact on the pathways following the priming step of inflammasome activation.

Selective inhibition of NLRP3 inflammasome by peptide originating from ASC^{PYD} domain

Furthermore, we were curious whether the peptides modulated other inflammasomes such as NLRC4 and AIM2. Upon treatment of iBMDMs with flagellin or poly (dA:dT) we observed that all modulatory peptides inhibited NLRC4 and AIM2 dependent IL-1β release (Fig. 4b) with the exception of ASC$^{PYD/H2\text{-}H3}$ which appeared to have no inhibitory effect. NLRP3 inflammasome inhibition was specific to the peptide amino acid sequence, as the scrambled version of ASC$^{PYD/H2\text{-}H3}$ no longer inhibited IL-1β maturation upon treatment of iBMDMs with particulate NLRP3 trigger alum (Fig. S7e).

In terms of other peptides ASC-derived ASC$^{CARD/H2\text{-}H3}$ significantly inhibited NLRC4 and AIM2 which was expected since its target site – caspase 1 is common to both NLRP3, NLRC4 and AIM2 inflammasome axes (Fig. 4b, d). However, contrary to our expectations, all of the effective NLRP3-derived peptides exhibited some effect on the NLRC4 and AIM2 inflammasomes. This might indicate certain extent of conservation within the regions in the inflammasomes or possible cooperation of these receptors as previously reported (56–58). To ensure that the peptides did not inhibit potential NLRP3 contribution within the flagellin-stimulated NLRC4 inflammasome, we repeated our experiments in NLRP3-deficient macrophages. Similarly, all of the NLRP3 derived peptides along with ASC$^{CARD/H2\text{-}H3}$ nearly eliminated the flagellin-stimulated IL-1β release thus further demonstrating inhibition that was not specific to NLRP3 while the ASC$^{PYD/H2\text{-}H3}$ peptide had no inhibitory effect (Fig. 4c). In conclusion, among the inhibitory peptide candidates ASC$^{PYD/H2\text{-}H3}$ peptide exhibited selective and sequence-specific inhibition of NLRP3 inflammasome activation while other peptides inhibited also NLRC4 and AIM2 inflammasomes.

ASC$^{PYD/H2\text{-}H3}$ binds NLRP3^{PYD} domain and crosses BBB when equipped with Angiopep-2 tag

Preclinical and clinical studies implicate NLRP3 inflammasome in a variety of neurodegenerative diseases (59). Those diseases still lack efficient therapy which makes the development of NLRP3 inflammasome inhibitors and their testing in clinical settings particularly interesting. Charged or large molecules such as peptides and proteins are notoriously difficult to transfer through the blood-brain barrier (BBB) (60). To follow whether NLRP3 inflammasome selective peptide can penetrate mouse brain we equipped the ASC$^{PYD/H2\text{-}H3}$ peptide with a short hydrophobic sequence from the Kunitz protease inhibitor domain (Angiopep-2). This motif is known to enable certain protease inhibitors such as aprotinin to bind the low density lipoprotein receptor

related protein (LPR) expressed on the vessel endothelium and subsequent transfer of the inhibitors through the BBB via transcytosis (61).

Firstly, we wanted to confirm that the addition of the Angiopep-2 sequence did not disrupt the inhibitory potential of the $ASC^{PYD/H2\text{-}H3}$ peptide. We treated microglia cells with particulate NLRP3 inflammasome instigator alum in the presence of the Angiopep2-$ASC^{PYD/H2\text{-}H3}$ peptide and observed that its inhibitory effect on IL-1β release is similar to that of $ASC^{PYD/H2\text{-}H3}$ (Fig. 5a). As $ASC^{PYD/H2\text{-}H3}$ selectively inhibited NLRP3 inflammasome, we suspected that it preferentially binds to $NLRP3^{PYD}$ domain. Correctly folded $NLRP3^{PYD}$-Histag was expressed in bacteria and its monomeric version purified (Fig. S8a-c). We then used surface plasmon resonance (SPR) to investigate whether the target of this peptide is $NLRP3^{PYD}$. $NLRP3^{PYD}$ domain was immobilized on sensor chip and increasing concentrations of the Angiopep2-$ASC^{PYD/H2\text{-}H3}$ analyte were injected. Although exact Kd value could not be determined as plateau response was not reached due to low solubility of the analyte (peptide), SPR data nevertheless revealed that the peptide specifically interacts with $NLRP3^{PYD}$ in micromolar concentrations (Fig. 5b).

Furthermore, to allow visualization of the Angiopep2-$ASC^{PYD/H2\text{-}H3}$ peptide and assess its ability to penetrate the microglial cell membrane and the BBB, the peptide was tagged with tetramethylrhodamine (Angiopep2-$ASC^{PYD/H2\text{-}H3}$-TMR). Angiopep2-$ASC^{PYD/H2\text{-}H3}$-TMR was able to cross the membrane and localize in the cytosol of microglial cells (Fig. 5c). We then evaluated its effectiveness at crossing the BBB *in vivo*. Mice were intravenously injected with the Angiopep2-$ASC^{PYD/H2\text{-}H3}$-TMR or the control $ASC^{PYD/H2\text{-}H3}$ peptide without the Angiopep-2 domain ($ASC^{PYD/H2\text{-}H3}$-TMR) and sacrificed after 1h or 3h. Histological analysis was performed on the brain and other internal organs to detect TMR fluorescence. While $ASC^{PYD/H2\text{-}H3}$-TMR only poorly localized in the brain and was predominantly detected in kidneys due to normal clearance of injected compounds, TMR fluorescence inside the brain was detected in the case of Angiopep2-$ASC^{PYD/H2\text{-}H3}$-TMR (Fig. 5d). As expected it was also detected in kidneys but not in any other internal organs showing a selective retention of Angiopep2-$ASC^{PYD/H2\text{-}H3}$-TMR inside the brain. Angiopep2-$ASC^{PYD/H2\text{-}H3}$-TMR was still detectable in the brain after 3h while $ASC^{PYD/H2\text{-}H3}$-TMR was already eliminated which further confirms the retention potential of $ASC^{PYD/H2\text{-}H3}$ equipped with Angiopep-2 motif (Fig. S8d).

Moreover, in addition to the Angiopep-2 tag, a peptide motif originating from the Antennapedia transcription factor from *Drosophila melanogaster* allowed the localization of the Antennapedia-$ASC^{PYD/H2\text{-}H3}$-TMR peptide in the brain tissue upon i.v. injection. *In vivo* imaging of mice, treated with Antennapedia-$ASC^{PYD/H2\text{-}H3}$-TMR revealed fluorescence in the head and upper back (Fig. S9a). Central nervous system localization was confirmed

by the histological analysis of collected internal organs upon sacrifice which revealed TMR fluorescence in the brain in case of Antennapedia-ASC$^{PYD/H2-H3}$-TMR (Fig. S9b). Together, these findings suggest that tagging of ASC$^{PYD/H2-H3}$ peptide with internalization tags does not compromise its activity in terms of inflammasome inhibition and that this peptide when equipped with either Angiopep-2 or Antennapedia tags efficiently crosses the blood-brain barrier.

Peptide ASC$^{PYD/H2-H3}$ effectively inhibits silica-induced peritonitis in murine model

Our cell-based results show that ASC$^{PYD/H2-H3}$ peptide inhibited NLRP3 inflammasome selectively and bound to the isolated NLRP3^{PYD} domain. For this reason we decided to test its effectiveness in murine silica-induced peritonitis model. Crystal or particle induced peritonitis has been previously shown to depend on NLRP3 (62). When mice were pretreated with intraperitoneally administered ASC$^{PYD/H2-H3}$ peptide, the number of peritoneally infiltrated neutrophils was markedly decreased in comparison to DMSO treated mice as determined by cytometric analysis (Fig. 6). This result shows that *in vivo* administered peptide ASC$^{PYD/H2-H3}$ is able to effectively suppress NLRP3-driven inflammation in mouse peritonitis model.

DISCUSSION

Large body of literature has linked NLRP3 inflammasome to various common diseases such as diabetes, occupational diseases (e.g. asbestosis) and rare genetic autoinflammatory syndromes, CAPS. Current therapy of CAPS relies on blocking IL-1 signaling, which is a downstream process common to various inflammasomes. Considerable disadvantages such as susceptibility of treated patients to infection have a sparked lively search for novel NLRP3 inflammasome inhibitors, which to-date include small molecules, plant metabolites, viral proteins and endogenous inflammasome regulators (for recent reviews the reader is referred to (59, 63, 64)). NLRP3 inflammasome represents a prototypic proinflammatory multiprotein complex which can be inhibited at different stages of assembly. In the present study we identified five peptides originating from segments of different domains that inhibit inflammasome at different stages and with different specificity.

NLRP3 oligomerization is the first stage of the inflammasome assembly. NLRP3 acts as an ATPase to support this step (65), thus several small molecules were identified to interfere with ATPase activity including IFN39 (22), OLT1177 (66) and CY-09 (21) which binds to Walker A motif. Sulfonylurea-based compound MCC950 (CRID3) (20) seems to be the most potent so far identified NLRP3 inflammasome inhibitor (21) which binds to Walker B motif (67–69). MCC950 was also extensively tested in preclinical models and entered phase II clinical trial for rheumatoid arthritis when liver toxicity was observed, however, relatively large dose was applied (63). Further direct NLRP3 inhibitors include oridonin, which was shown to bind Cys279 in

NLRP3^{NACHT} domain and abrogate NLRP3-NEK7 interaction (70). Although NLRP3 plays a role in the initial stage of inflammasome assembly, the peptides from NLRP3^{NACHT} domain either exhibited no modulation or were broad inhibitors of inflammasomes and/or NF-κB. The lack of modulation of peptides NLRP3^{WalkerA}, NLRP3$^{(250-265)}$, NLRP3$^{(427-447)}$ and NLRP3$^{(560-593)}$ suggests that these segments are not a part of NLRP3 oligomerization surface, but according to the published NLRP3 structure (31), CAPS-associated mutations in those segments might stabilize interdomain interface and thus inactive NLRP3 conformation. In spite of expectations, NLRP3^{WalkerB} peptide is a broad inflammasome and NF-κB inhibitor. NLRP3^{Sensor1} peptide and NLRP3$^{PYD/H2-H3}$ inhibited all inflammasomes while modulating NF-κB only at the highest concentration. However, even direct NLRP3 inhibitors that are selective for NLRP3 inflammasome can exhibit multi-target effects. Tranilast, which is an approved anti-allergic drug, was shown to directly bind NLRP3^{NACHT} domain and prevent NLRP3 oligomerization (23), yet some effects on expression of proinflammatory cytokines pro-IL-1β and IL-6 were also observed.

Peptides from interaction domains NLRP3$^{PYD/H2-H3}$, ASC$^{PYD/H2-H3}$ and ASC$^{CARD/H2-H3}$ were chosen to inhibit PYD-PYD and CARD-CARD interactions, which are further steps in inflammasome assembly. In humans, these interactions are targeted by endogenous modulators of inflammasome assembly comprising isolated pyrin domains or CARD domains, POPs (PYD only proteins) and COPs (CARD only proteins). As demonstrated for peptides in this study, POPs were shown to exhibit different selectivity. POP1 and POP2 bind ASC and are broad inflammasome inhibitors (71–76). POP3 on the other hand specifically inhibits ALR inflammasomes (77). Broad inflammasome inhibition with NLRP3$^{PYD/H2-H3}$ suggests that it acts on ASC similarly as POP1 and POP2.

Selective inhibition of NLRP3 inflammasome was achieved by ASC$^{PYD/H2-H3}$ peptide through binding to the NLRP3^{PYD}. This region was previously suggested to support binding of NLRP3^{PYD} (76). Although this segment of ASC is involved in all three types of interface in the ASC^{PYD} filament (30) and ASC^{PYD} interactions are (despite lower Kd) governed by the same amino acid residues as ASC^{PYD}-NLRP3^{PYD} interactions (78), the effect on other inflammasomes that engage ASC was not observed. Thus selectivity of this peptide suggests that the peptide cannot efficiently inhibit ASC^{PYD} polymerization or bind pyrin domains of ASC or AIM2.

Current knowledge on CARD-only proteins is based on *in vitro* studies. INCA was found at the top of pro-caspase-1 CARD filaments thus preventing CARD-CARD interactions between ASC and pro-caspase-1 (79). While COPs sequence is similar to pro-caspase-1 CARD, we tested H2-H3 segment of ASC, which participates in two out of three types of interactions in ASC^{CARD} filament (47). Inhibition of ASC oligomerization observed

by $ASC^{CARD/H2-H3}$ is in agreement with studies which showed that mutations in this region interfere with ASC speck formation (32). As the same region was shown to be crucial for binding of pro-caspase-1 (48), the effects of $ASC^{CARD/H2-H3}$ on the recruitment of pro-caspase-1 cannot be excluded. Interestingly, a nanobody against ASC was developed which inhibited ASC speck condensation and cytokine maturation downstream of various inflammasomes. This nanobody binds a hydrophobic patch in H6 at the end of ASC^{CARD} domain (33). The variety of interactions formed by different domains that govern inflammasome assembly suggest that a variety of peptides and their combinations might be used for modulation of inflammasome assembly.

As inflammation in the central nervous system is one of the most interesting targets of inflammasome inhibitors, molecules that efficiently cross the blood-brain barrier are needed. Clinically used IL-1 signaling antagonists anakinra, rilonacept and canakinumab penetrate the brain poorly. It was shown that only 0.3 % of peripheral serum concentration of anakinra can be found in the brains of non-human primates (80). In current study, two different peptide tags enabled $ASC^{PYD/H2-H3}$ to cross the blood-brain barrier in a mouse model. While the degradation problems kept the popularity of peptides as therapeutic agents at bay, new advances in the field of targeted delivery and drug formulation enabled their revival. A possible strategy for stabilization could be so called stapling (81) and stapled peptides were shown to inhibit ASC polymerization (82). We further demonstrate the functionality of $ASC^{PYD/H2-H3}$ in mouse peritonitis model, which supports further exploration of peptide-based therapeutics for modulation of inflammasome or similar supramolecular organizing centers. Otherwise, peptide-based compounds have a long history as irreversible inhibitors of caspases (83) and peptides were also used to target other inflammatory signaling pathways (84, 85). This study shows that peptides are valuable tools for studying assembly of macromolecular complexes as well as for targeting those complexes *in vivo* even in protected regions such as the brain.

In conclusion, selected peptides corresponding to segments of NLRP3 and ASC which markedly reduced NLRP3 inflammasome activation in response to diverse NLRP3 inflammasome instigators could represent a technical toolbox for research of individual stages of inflammasome assembly as well as the starting ground for developing novel therapeutic approaches towards chronic inflammation that significantly aids in progression of several debilitating pathologies such as neurodegeneration.

ACKNOWLEDGEMENTS

This work was funded by the Slovenian Research Agency (J3-5503, J3-6791, J3-1746 to I.H.B, core funding P4-176, Z3-9276 to D.L. and Young Researcher grant to P.S.). I.H.B. is a recipient of the ICGEB grant (CRP-SVN18-01). The authors would like to thank Roman Jerala for fruitful discussions, to Robert Bremšak, Irena

Škraba, Darija Oven and Jure Prešeren for technical support and to student Kaja Klemenc for technical help with the experiments. The authors are grateful to Kate A. Fitzgerald and Douglas Golenbock (University of Massachusetts Medical School, USA) for providing immortalized mouse macrophages and microglia.

AUTHOR CONTRIBUTIONS

P.S. performed the majority of experiments, analyzed data and wrote the manuscript, D.L. performed animal study, Ž.S. and V.H. performed experiments, G.A. oversaw the SPR study and helped with writing of the manuscript, I.H.B. designed the study, oversaw the study and wrote the manuscript.

REFERENCES

1. Kayagaki, N., Stowe, I. B., Lee, B. L., O'Rourke, K., Anderson, K., Warming, S., Cuellar, T., Haley, B., Roose-Girma, M., Phung, Q. T., Liu, P. S., Lill, J. R., Li, H., Wu, J., Kummerfeld, S., Zhang, J., Lee, W. P., Snipas, S. J., Salvesen, G. S., Morris, L. X., Fitzgerald, L., Zhang, Y., Bertram, E. M., Goodnow, C. C., and Dixit, V. M. (2015) Caspase-11 cleaves gasdermin D for non-canonical inflammasome signalling. *Nature* **526**, 666–671

2. Shi, J., Zhao, Y., Wang, K., Shi, X., Wang, Y., Huang, H., Zhuang, Y., Cai, T., Wang, F., and Shao, F. (2015) Cleavage of GSDMD by inflammatory caspases determines pyroptotic cell death. *Nature* **526**, 660–665

3. Evavold, C. L., Ruan, J., Tan, Y., Xia, S., Wu, H., and Kagan, J. C. (2018) The Pore-Forming Protein Gasdermin D Regulates Interleukin-1 Secretion from Living Macrophages. *Immunity* **48**, 35-44.e6

4. Evavold, C. L. and Kagan, J. C. (2019) Inflammasomes: Threat-Assessment Organelles of the Innate Immune System. *Immunity* **51**, 609–624

5. Vandanmagsar, B., Youm, Y.-H., Ravussin, A., Galgani, J. E., Stadler, K., Mynatt, R. L., Ravussin, E., Stephens, J. M., and Dixit, V. D. (2011) The NLRP3 inflammasome instigates obesity-induced inflammation and insulin resistance. *Nat. Med.* **17**, 179–188

6. Lee, H.-M., Kim, J.-J., Kim, H. J., Shong, M., Ku, B. J., and Jo, E.-K. (2013) Upregulated NLRP3 Inflammasome Activation in Patients With Type 2 Diabetes. *Diabetes* **62**, 194–204

7. Heneka, M. T., Kummer, M. P., Stutz, A., Delekate, A., Schwartz, S., Vieira-Saecker, A., Griep, A., Axt, D., Remus, A., Tzeng, T. C., Gelpi, E., Halle, A., Korte, M., Latz, E., and Golenbock, D. T. (2013) NLRP3 is activated in Alzheimer's disease and contributes to pathology in APP/PS1 mice. *Nature* **493**,

674–678

8. Venegas, C. and Heneka, M. T. (2019) Inflammasome-mediated innate immunity in Alzheimer's disease. *FASEB J.* fj.201900439

9. Youm, Y. H., Grant, R. W., McCabe, L. R., Albarado, D. C., Nguyen, K. Y., Ravussin, A., Pistell, P., Newman, S., Carter, R., Laque, A., Münzberg, H., Rosen, C. J., Ingram, D. K., Salbaum, J. M., and Dixit, V. D. (2013) Canonical Nlrp3 inflammasome links systemic low-grade inflammation to functional decline in aging. *Cell Metab.* **18**, 519–532

10. Touitou, I., Lesage, S., McDermott, M., Cuisset, L., Hoffman, H., Dode, C., Shoham, N., Aganna, E., Hugot, J. P., Wise, C., Waterham, H., Pugnere, D., Demaille, J., and De Menthiere, C. S. (2004) Infevers: An evolving mutation database for auto-inflammatory syndromes. *Hum. Mutat.* **24**, 194–198

11. Mariathasan, S., Weiss, D. S., Newton, K., McBride, J., O'Rourke, K., Roose-Girma, M., Lee, W. P., Weinrauch, Y., Monack, D. M., and Dixit, V. M. (2006) Cryopyrin activates the inflammasome in response to toxins and ATP. *Nature* **440**, 228–232

12. Dostert, C., Pétrilli, V., Bruggen, R. Van, Steele, C., Mossman, B. T., and Tschopp, J. (2008) Asbestos and Silica. *Science (80-.).* **674**, 674–677

13. Hornung, V., Bauernfeind, F., Halle, A., Samstad, E. O., Kono, H., Rock, K. L., Fitzgerald, K. A., and Latz, E. (2008) Silica crystals and aluminum salts activate the NALP3 inflammasome through phagosomal destabilization. *Nat. Immunol.* **9**, 847–856

14. Hafner-Bratkovič, I., Benčina, M., Fitzgerald, K. A., Golenbock, D., and Jerala, R. (2012) NLRP3 inflammasome activation in macrophage cell lines by prion protein fibrils as the source of IL-1β and neuronal toxicity. *Cell. Mol. Life Sci.* **69**, 4215–4228

15. Halle, A., Hornung, V., Petzold, G. C., Stewart, C. R., Monks, B. G., Reinheckel, T., Fitzgerald, K. A., Latz, E., Moore, K. J., and Golenbock, D. T. (2008) The NALP3 inflammasome is involved in the innate immune response to amyloid-beta. *Nat. Immunol.* **9**, 857–865

16. Muñoz-Planillo, R., Kuffa, P., Martínez-Colón, G., Smith, B., Rajendiran, T., and Núñez, G. (2013) K+ Efflux Is the Common Trigger of NLRP3 Inflammasome Activation by Bacterial Toxins and Particulate Matter. *Immunity* **38**

17. Hafner-Bratkovič, I. and Pelegrín, P. (2018) Ion homeostasis and ion channels in NLRP3 inflammasome activation and regulation. *Curr. Opin. Immunol.* **52**, 8–17

18. Pétrilli, V., Papin, S., Dostert, C., Mayor, A., Martinon, F., and Tschopp, J. (2007) Activation of the NALP3 inflammasome is triggered by low intracellular potassium concentration. *Cell Death Differ.* **14**, 1583–1589

19. Dinarello, C. A. and van der Meer, J. W. M. (2013) Treating inflammation by blocking interleukin-1 in humans. *Semin. Immunol.* **25**, 469–484

20. Coll, R. C., Robertson, A. A. B., Chae, J. J., Higgins, S. C., Muñoz-Planillo, R., Inserra, M. C., Vetter, I., Dungan, L. S., Monks, B. G., Stutz, A., Croker, D. E., Butler, M. S., Haneklaus, M., Sutton, C. E., Núñez, G., Latz, E., Kastner, D. L., Mills, K. H. G., Masters, S. L., Schroder, K., Cooper, M. A., and O'Neill, L. A. J. (2015) A small-molecule inhibitor of the NLRP3 inflammasome for the treatment of inflammatory diseases. *Nat. Med.* **21**, 248–255

21. Jiang, H., He, H., Chen, Y., Huang, W., Cheng, J., Ye, J., Wang, A., Tao, J., Wang, C., Liu, Q., Jin, T., Jiang, W., Deng, X., and Zhou, R. (2017) Identification of a selective and direct NLRP3 inhibitor to treat inflammatory disorders. *J. Exp. Med.* **214**, 3219–3238

22. Cocco, M., Pellegrini, C., Martinez-Banaclocha, H., Giorgis, M., Marini, E., Costale, A., Miglio, G., Fornai, M., Antonioli, L., Lopez-Castejon, G., Tapia-Abellan, A., Angosto, D., Hafner-Bratkovic, I., Regazzoni, L., Blandizzi, C., Pelegrin, P., and Bertinaria, M. (2017) Development of an Acrylate Derivative Targeting the NLRP3 Inflammasome for the Treatment of Inflammatory Bowel Disease. *J. Med. Chem.* **60**, 3656–3671

23. Huang, Y., Jiang, H., Chen, Y., Wang, X., Yang, Y., Tao, J., Deng, X., Liang, G., Zhang, H., Jiang, W., and Zhou, R. (2018) Tranilast directly targets NLRP3 to treat inflammasome-driven diseases. *EMBO Mol. Med.* **10**, e8689

24. Zorman, J., Sušjan, P., and Hafner-Bratkovič, I. (2016) Shikonin Suppresses NLRP3 and AIM2 Inflammasomes by Direct Inhibition of Caspase-1. *PLoS One* **11**, e0159826

25. Juliana, C., Fernandes-Alnemri, T., Wu, J., Datta, P., Solorzano, L., Yu, J. W., Meng, R., Quong, A. A., Latz, E., Scott, C. P., and Alnemri, E. S. (2010) Anti-inflammatory compounds parthenolide and bay 11-7082 are direct inhibitors of the inflammasome. *J. Biol. Chem.* **285**, 9792–9802

26. Chang, Y. P., Ka, S. M., Hsu, W. H., Chen, A., Chao, L. K., Lin, C. C., Hsieh, C. C., Chen, M. C., Chiu, H. W., Ho, C. L., Chiu, Y. C., Liu, M. L., and Hua, K. F. (2015) Resveratrol inhibits NLRP3 inflammasome activation by preserving mitochondrial integrity and augmenting autophagy. *J. Cell.*

Physiol. **230**, 1567–1579

27. Kagan, J. C., Magupalli, V. G., and Wu, H. (2014) SMOCs: supramolecular organizing centres that control innate immunity. *Nat. Rev. Immunol.* **14**, 821–826

28. Tan, Y. and Kagan, J. C. (2019) Innate Immune Signaling Organelles Display Natural and Programmable Signaling Flexibility. *Cell* **177**, 384-398.e11

29. Hafner-Bratkovič, I. (2017) Prions, prionoid complexes and amyloids: The bad, the good and something in between. *Swiss Med. Wkly.* **147**

30. Lu, A., Magupalli, V. G., Ruan, J., Yin, Q., Atianand, M. K., Vos, M. R., Schr??der, G. F., Fitzgerald, K. A., Wu, H., and Egelman, E. H. (2014) Unified polymerization mechanism for the assembly of asc-dependent inflammasomes. *Cell* **156**, 1193–1206

31. Sharif, H., Wang, L., Wang, W. L., Magupalli, V. G., Andreeva, L., Qiao, Q., Hauenstein, A. V, Wu, Z., Núñez, G., Mao, Y., and Wu, H. (2019) Structural mechanism for NEK7-licensed activation of NLRP3 inflammasome. *Nature* **570**, 338–343

32. Dick, M. S., Sborgi, L., Rühl, S., Hiller, S., and Broz, P. (2016) ASC filament formation serves as a signal amplification mechanism for inflammasomes. *Nat. Commun.* **7**

33. Schmidt, F. I., Lu, A., Chen, J. W., Ruan, J., Tang, C., Wu, H., and Ploegh, H. L. (2016) A single domain antibody fragment that recognizes the adaptor ASC defines the role of ASC domains in inflammasome assembly. *J. Exp. Med.* **213**, 771–790

34. De Nardo, D., Labzin, L. I., Kono, H., Seki, R., Schmidt, S. V, Beyer, M., Xu, D., Zimmer, S., Lahrmann, C., Schildberg, F. A., Vogelhuber, J., Kraut, M., Ulas, T., Kerksiek, A., Krebs, W., Bode, N., Grebe, A., Fitzgerald, M. L., Hernandez, N. J., Williams, B. R. G., Knolle, P., Kneilling, M., Röcken, M., Lütjohann, D., Wright, S. D., Schultze, J. L., and Latz, E. (2014) High-density lipoprotein mediates anti-inflammatory reprogramming of macrophages via the transcriptional regulator ATF3. *Nat. Immunol.* **15**, 152–160

35. Baroja-Mazo, A., Martín-Sánchez, F., Gomez, A. I., Martínez, C. M., Amores-Iniesta, J., Compan, V., Barberà-Cremades, M., Yagüe, J., Ruiz-Ortiz, E., Antón, J., Buján, S., Couillin, I., Brough, D., Arostegui, J. I., and Pelegrín, P. (2014) The NLRP3 inflammasome is released as a particulate danger signal that amplifies the inflammatory response. *Nat. Immunol.* **15**, 738–748

36. Venegas, C., Kumar, S., Franklin, B. S., Dierkes, T., Brinkschulte, R., Tejera, D., Vieira-Saecker, A.,

Schwartz, S., Santarelli, F., Kummer, M. P., Griep, A., Gelpi, E., Beilharz, M., Riedel, D., Golenbock, D. T., Geyer, M., Walter, J., Latz, E., and Heneka, M. T. (2017) Microglia-derived ASC specks cross-seed amyloid-β in Alzheimer's disease. *Nature* **552**, 355–361

37. Doig, A. J. and Derreumaux, P. (2015) Inhibition of protein aggregation and amyloid formation by small molecules. *Curr. Opin. Struct. Biol.* **30**, 50–56

38. Hafner-Bratkovič, I., Sušjan, P., Lainšček, D., Tapia-Abellán, A., Cerović, K., Kadunc, L., Angosto-Bazarra, D., Pelegrín, P., and Jerala, R. (2018) NLRP3 lacking the leucine-rich repeat domain can be fully activated via the canonical inflammasome pathway. *Nat. Commun.* **9**

39. Ahn, H., Kim, J., Jeung, E.-B., and Lee, G.-S. (2014) Dimethyl sulfoxide inhibits NLRP3 inflammasome activation. *Immunobiology* **219**, 315–322

40. Forstnerič, V., Ivičak-Kocjan, K., Plaper, T., Jerala, R., and Benčina, M. (2017) The role of the C-terminal D0 domain of flagellin in activation of Toll like receptor 5. *PLoS Pathog.* **13**

41. de Alba, E. (2009) Structure and interdomain dynamics of apoptosis-associated speck-like protein containing a CARD (ASC). *J. Biol. Chem.* **284**, 32932–32941

42. Chu, L. H., Gangopadhyay, A., Dorfleutner, A., and Stehlik, C. (2015) An updated view on the structure and function of PYRIN domains. *Apoptosis* **20**, 157–173

43. de Alba, E. (2019) Structure, interactions and self-assembly of ASC-dependent inflammasomes. *Arch. Biochem. Biophys.* **670**, 15–31

44. Bae, J. Y. and Park, H. H. (2011) Crystal structure of NALP3 Protein Pyrin Domain (PYD) and its implications in inflammasome assembly. *J. Biol. Chem.* **286**, 39528–39536

45. Cai, X., Chen, J., Xu, H., Liu, S., Jiang, Q.-X., Halfmann, R., and Chen, Z. J. (2014) Prion-like polymerization underlies signal transduction in antiviral immune defense and inflammasome activation. *Cell* **156**, 1207–1222

46. Sborgi, L., Ravotti, F., Dandey, V. P., Dick, M. S., Mazur, A., Reckel, S., Chami, M., Scherer, S., Huber, M., Böckmann, A., Egelman, E. H., Stahlberg, H., Broz, P., Meier, B. H., and Hiller, S. (2015) Structure and assembly of the mouse ASC inflammasome by combined NMR spectroscopy and cryo-electron microscopy. *Proc. Natl. Acad. Sci.*

47. Li, Y., Fu, T.-M., Lu, A., Witt, K., Ruan, J., Shen, C., and Wu, H. (2018) Cryo-EM structures of ASC

and NLRC4 CARD filaments reveal a unified mechanism of nucleation and activation of caspase-1. *Proc. Natl. Acad. Sci.*

48. Proell, M., Gerlic, M., Mace, P. D., Reed, J. C., and Riedl, S. J. (2013) The CARD plays a critical role in ASC foci formation and inflammasome signalling. *Biochem. J.* **449**, 613–621

49. Sušjan, P., Roškar, S., and Hafner-Bratkovič, I. (2017) The mechanism of NLRP3 inflammasome initiation: Trimerization but not dimerization of the NLRP3 pyrin domain induces robust activation of IL-1β. *Biochem. Biophys. Res. Commun.* **483**, 823–828

50. Zhang, L., Chen, S., Ruan, J., Wu, J., Tong, A. B., Yin, Q., Li, Y., David, L., Lu, A., Wang, W. L., Marks, C., Ouyang, Q., Zhang, X., Mao, Y., and Wu, H. (2015) Cryo-EM structure of the activated NAIP2-NLRC4 inflammasome reveals nucleated polymerization. *Science (80-.).* **350**, 404–409

51. Hu, Z., Zhou, Q., Zhang, C., Fan, S., Cheng, W., Zhao, Y., Shao, F., Wang, H.-W., Sui, S.-F., and Chai, J. (2015) Structural and biochemical basis for induced self-propagation of NLRC4. *Science (80-.).* **350**, 399–404

52. Van Gijn, M. E., Ceccherini, I., Shinar, Y., Carbo, E. C., Slofstra, M., Arostegui, J. I., Sarrabay, G., Rowczenio, D., Omoyımnı, E., Balci-Peynircioglu, B., Hoffman, H. M., Milhavet, F., Swertz, M. A., and Touitou, I. (2018) New workflow for classification of genetic variants' pathogenicity applied to hereditary recurrent fevers by the International Study Group for Systemic Autoinflammatory Diseases (INSAID). *J. Med. Genet.* **55**, 530–537

53. Macdonald, J. A., Wijekoon, C. P., Liao, K. C., and Muruve, D. A. (2013) Biochemical and structural aspects of the ATP-binding domain in inflammasome-forming human NLRP proteins. *IUBMB Life* **65**, 851–862

54. Nelson, A. R., Borland, L., Allbritton, N. L., and Sims, C. E. (2007) Myristoyl-based transport of peptides into living cells. *Biochemistry* **46**, 14771–14781

55. Jerala, R. and Porro, M. (2004) Endotoxin neutralizing peptides. *Curr. Top. Med. Chem.* **4**, 1173–1184

56. Man, S. M., Hopkins, L. J., Nugent, E., Cox, S., Gluck, I. M., Tourlomousis, P., Wright, J. A., Cicuta, P., Monie, T. P., and Bryant, C. E. (2014) Inflammasome activation causes dual recruitment of NLRC4 and NLRP3 to the same macromolecular complex. *Proc. Natl. Acad. Sci.* **111**, 7403–7408

57. Gambin, Y., Giles, N., O'Carroll, A., Polinkovsky, M., Hunter, D., and Sierecki, E. (2017) Single-molecule fluorescence reveals the oligomerisation and folding steps driving the prion-like behaviour of

ASC. *J. Mol. Biol.*

58. Qu, Y., Misaghi, S., Newton, K., Maltzman, A., Izrael-Tomasevic, A., Arnott, D., and Dixit, V. M. (2016) NLRP3 recruitment by NLRC4 during Salmonella infection. *J. Exp. Med.* **213**, 877–885

59. Voet, S., Srinivasan, S., Lamkanfi, M., and Van Loo, G. (2019) Inflammasomes in neuroinflammatory and neurodegenerative diseases. *EMBO Mol Med* **11**, 10248

60. Pardridge, W. M. (2005) The blood-brain barrier: bottleneck in brain drug development. *NeuroRx* **2**, 3–14

61. Demeule, M., Regina, A., Che, C., Poirier, J., Nguyen, T., Gabathuler, R., Castaigne, J.-P., and Beliveau, R. (2007) Identification and Design of Peptides as a New Drug Delivery System for the Brain. *J. Pharmacol. Exp. Ther.* **324**, 1064–1072

62. Duewell, P., Kono, H., Rayner, K. J., Sirois, C. M., Vladimer, G., Bauernfeind, F. G., Abela, G. S., Franchi, L., Nuñez, G., Schnurr, M., Espevik, T., Lien, E., Fitzgerald, K. A., Rock, K. L., Moore, K. J., Wright, S. D., Hornung, V., and Latz, E. (2010) NLRP3 inflammasomes are required for atherogenesis and activated by cholesterol crystals. *Nature* **464**, 1357–1361

63. Mangan, M. S. J., Olhava, E. J., Roush, W. R., Seidel, H. M., Glick, G. D., and Latz, E. (2018) Targeting the NLRP3 inflammasome in inflammatory diseases. *Nat. Rev. Drug Discov.* **17**, 688

64. Swanson, K. V, Deng, M., and Ting, J. P.-Y. (2019) The NLRP3 inflammasome: molecular activation and regulation to therapeutics. *Nat. Rev. Immunol.* **19**, 477–489

65. Duncan, J. A., Bergstralh, D. T., Wang, Y., Willingham, S. B., Ye, Z., Zimmermann, A. G., and Ting, J. P.-Y. (2007) Cryopyrin/NALP3 binds ATP/dATP, is an ATPase, and requires ATP binding to mediate inflammatory signaling. *Proc. Natl. Acad. Sci.* **104**, 8041–8046

66. Marchetti, C., Swartzwelter, B., Gamboni, F., Neff, C. P., Richter, K., Azam, T., Carta, S., Tengesdal, I., Nemkov, T., D'Alessandro, A., Henry, C., Jones, G. S., Goodrich, S. A., St. Laurent, J. P., Jones, T. M., Scribner, C. L., Barrow, R. B., Altman, R. D., Skouras, D. B., Gattorno, M., Grau, V., Janciauskiene, S., Rubartelli, A., Joosten, L. A. B., and Dinarello, C. A. (2018) OLT1177, a β-sulfonyl nitrile compound, safe in humans, inhibits the NLRP3 inflammasome and reverses the metabolic cost of inflammation. *Proc. Natl. Acad. Sci. U. S. A.* **115**, E1530–E1539

67. Tapia-Abellán, A., Angosto-Bazarra, D., Martínez-Banaclocha, H., de Torre-Minguela, C., Cerón-Carrasco, J. P., Pérez-Sánchez, H., Arostegui, J. I., and Pelegrin, P. (2019) MCC950 closes the active

conformation of NLRP3 to an inactive state. *Nat. Chem. Biol.* **15**, 560–564

68. Coll, R. C., Hill, J. R., Day, C. J., Zamoshnikova, A., Boucher, D., Massey, N. L., Chitty, J. L., Fraser, J. A., Jennings, M. P., Robertson, A. A. B., and Schroder, K. (2019) MCC950 directly targets the NLRP3 ATP-hydrolysis motif for inflammasome inhibition. *Nat. Chem. Biol.* **15**, 556–559

69. Vande Walle, L., Stowe, I. B., Šácha, P., Lee, B. L., Demon, D., Fossoul, A., Van Hauwermeiren, F., Saavedra, P. H. V., Šimon, P., Šubrt, V., Kostka, L., Stivala, C. E., Pham, V. C., Staben, S. T., Yamazoe, S., Konvalinka, J., Kayagaki, N., and Lamkanfi, M. (2019) MCC950/CRID3 potently targets the NACHT domain of wild-type NLRP3 but not disease-associated mutants for inflammasome inhibition. *PLOS Biol.* **17**, e3000354

70. He, H., Jiang, H., Chen, Y., Ye, J., Wang, A., Wang, C., Liu, Q., Liang, G., Deng, X., Jiang, W., and Zhou, R. (2018) Oridonin is a covalent NLRP3 inhibitor with strong anti-inflammasome activity. *Nat. Commun.* **9**

71. Ratsimandresey, R. A., Chu, L. H., Khare, S., de Almeida, L., Gangopadhyay, A., Indramohan, M., Misharin, A. V., Greaves, D. R., Perlman, H., Dorfleutner, A., and Stehlik, C. (2017) The PYRIN domain-only protein POP2 inhibits inflammasome priming and activation. *Nat. Commun.* **8**, 15556

72. Periasamy, S., Porter, K. A., Atianand, M. K., Le, H. T., Earley, S., Duffy, E. B., Haller, M. C., Chin, H., and Harton, J. A. (2017) Pyrin-only protein 2 limits inflammation but improves protection against bacteria. *Nat. Commun.* **8**

73. Atianand, M. K., Fuchs, T., and Harton, J. A. (2011) Recent evolution of the NF-κB and inflammasome regulating protein POP2 in primates. *BMC Evol. Biol.* **11**, 56

74. Bedoya, F., Sandler, L. L., and Harton, J. A. (2007) Pyrin-Only Protein 2 Modulates NF-κB and Disrupts ASC:CLR Interactions. *J. Immunol.* **178**, 3837–3845

75. de Almeida, L., Khare, S., Misharin, A. V, Patel, R., Ratsimandresey, R. A., Wallin, M. C., Perlman, H., Greaves, D. R., Hoffman, H. M., Dorfleutner, A., and Stehlik, C. (2015) The PYRIN Domain-only Protein POP1 Inhibits Inflammasome Assembly and Ameliorates Inflammatory Disease. *Immunity* **43**, 264–276

76. Srimathi, T., Robbins, S. L., Dubas, R. L., Chang, H., Cheng, H., Roder, H., and Young, C. P. (2008) Mapping of POP1-binding site on pyrin domain of ASC. *J. Biol. Chem.* **283**, 15390–15398

77. Khare, S., Ratsimandresey, R. a, de Almeida, L., Cuda, C. M., Rellick, S. L., Misharin, A. V, Wallin, M.

C., Gangopadhyay, A., Forte, E., Gottwein, E., Perlman, H., Reed, J. C., Greaves, D. R., Dorfleutner, A., and Stehlik, C. (2014) The PYRIN domain-only protein POP3 inhibits ALR inflammasomes and regulates responses to infection with DNA viruses. *Nat. Immunol.* **15**, 343–353

78. Oroz, J., Barrera-Vilarmau, S., Alfonso, C., Rivas, G., and De Alba, E. (2016) ASC pyrin domain self-associates and binds NLRP3 protein using equivalent binding interfaces∗. *J. Biol. Chem.* **291**, 19487–19501

79. Lu, A., Li, Y., Schmidt, F. I., Yin, Q., Chen, S., Fu, T. M., Tong, A. B., Ploegh, H. L., Mao, Y., and Wu, H. (2016) Molecular basis of caspase-1 polymerization and its inhibition by a new capping mechanism. *Nat. Struct. Mol. Biol.* **23**, 416–425

80. Fox, E., Jayaprakash, N., Pham, T.-H., Rowley, A., McCully, C. L., Pucino, F., and Goldbach-Mansky, R. (2010) The serum and cerebrospinal fluid pharmacokinetics of anakinra after intravenous administration to non-human primates. *J. Neuroimmunol.* **223**, 138–140

81. Walensky, L. D. and Bird, G. H. (2014) Hydrocarbon-stapled peptides: principles, practice, and progress. *J. Med. Chem.* **57**, 6275–6288

82. Pal, A., Neo, K., Rajamani, L., Ferrer, F. J., Lane, D. P., Verma, C. S., and Mortellaro, A. (2019) Inhibition of NLRP3 inflammasome activation by cell-permeable stapled peptides. *Sci. Rep.* **9**

83. Kudelova, J., Fleischmannova, J., Adamova, E., and Matalova, E. (2015) Pharmacological caspase inhibitors: research towards therapeutic perspectives. *J. Physiol. Pharmacol.* **66**, 473–482

84. Lysakova-Devine, T., Keogh, B., Harrington, B., Nagpal, K., Halle, A., Golenbock, D. T., Monie, T., and Bowie, A. G. (2010) Viral Inhibitory Peptide of TLR4, a Peptide Derived from Vaccinia Protein A46, Specifically Inhibits TLR4 by Directly Targeting MyD88 Adaptor-Like and TRIF-Related Adaptor Molecule. *J. Immunol.* **185**, 4261–4271

85. Avbelj, M., Horvat, S., and Jerala, R. (2011) The Role of Intermediary Domain of MyD88 in Cell Activation and Therapeutic Inhibition of TLRs. *J. Immunol.* **187**, 2394–2404

FIGURE DESCRIPTIONS

Figure 1 Peptides derived from PYD and CARD interaction domains of NLRP3 and ASC inhibit IL-1β secretion in iBMDMs

a – Schematic representation of key interactions governing inflammasome assembly with the list of selected peptides.
b – IL-1β levels by ELISA assay after iBMDMs were primed with 100 ng/mL LPS for 6 h, exposed to peptides (1, 5, 10, 20, 40 μM) or DMSO (concentration equivalent to the one present at highest peptide concentration) for 0.5 h before the addition of 200 μg/mL nanoSiO_2 for 4 h. IL-1β ELISA was performed on supernatants. Numbers were normalized to non-peptide-treated mean value, which represents 100% stimulation. Normalized mean values and standard deviations of at least two repeats are shown. Results are representative of 3 independent experiments.

Figure 2 Peptides attenuate ATP-induced and constitutive CAPS-associated activation

a – IL-1β levels by ELISA assay after iBMDMs were primed with 100 ng/mL LPS for 6 h, exposed to peptides (10, 20, 30, in charts in the bottom row also 40 μM) or DMSO (concentration equivalent to the one present at highest peptide concentration) for 0.5 h before the addition of 5 mM ATP for 1 h. Numbers were normalized to non-peptide-treated mean value, which represents 100% stimulation. Normalized mean values and standard deviations of at least two repeats are shown. Results are representative of 3 independent experiments.
b – Metabolic activity of iBMDMs as determined by XTT assay after treatment as above with 1, 5, 10, 20, 30, 40 μM peptides or DMSO (concentration equivalent to the one present at highest peptide concentration). Normalized mean values and standard deviations of at least two repeats are shown. Results are representative of 2 independent experiments.
c – IL-1β levels by ELISA assay after iBMDMs with CAPS mutations were pretreated with peptides (20, 40 μM) for 0.5 h and then activated with 100 ng/mL LPS and 0.6 μg/mL doxycycline for 9 h. Mean values and standard deviations of at least two repeats are shown. Results are representative of 2 independent experiments.

Figure 3 Inhibitory peptides attenuate caspase-1 activation and ASC oligomerization

a – Caspase-1 levels as determined by flow cytometry with FAM-FLICA reagent after iBMDMs that were pretreated with 30 μM peptides or DMSO (at concentration equivalent to the one present at highest peptide concentration) for 0.5 h were activated with 100 ng/mL LPS and 5 μM nigericin for 2.5 h. Results are representative of 2 independent experiments.
b,c – Immunofluorescently stained ASC specks after iBMDMs were primed with 100 ng/mL LPS for 6 h and exposed to 40 μM peptides or DMSO for 0.5 h before the addition of 190 ng/mL nanoSiO_2 for 4h. Cells were subsequently fixed, permeabilized and immunofluorescently stained for ASC (AlexaFluor488, green) and nuclei (DAPI, blue). We show representative images (b) and mean speck/nuclei ratio with standard deviations based on the quantification of at least 6 confocal microscopy images for each treatment (c). Adjustments were made in

brightness and contrast in LAS AF and images cropped in ImageJ. Results are a representative of 2 independent experiments. Scale bar = 30 μm.

Figure 4 The effect of peptides on the NF-κB and NLRC4 and AIM2 inflammasomes

a – SEAP levels with QUANTI-Blue assay after RAWBlue cells were exposed to peptides (5, 10, 15, 30 μM – left and 1, 5, 10, 20, 40 μM – right) or DMSO for 0.5 h before overnight stimulation with 50 ng/mL LPS. Mean absorbance at 630 nm and standard deviations of at least two repeats are shown. Results are representative of 2 independent experiments.

b – IL-1β levels by ELISA assay after iBMDMs were primed with 100 ng/mL LPS for 6 h, exposed to peptides (5,10,20, 40 μM) or DMSO for 0.5 h before transfection of 1000 μg/mL flagellin/DOTAP for 4 h. Mean values and standard deviations of at least two repeats are shown. Results are representative of 2 independent experiments.

c – IL-1β levels by ELISA assay after NLRP3$^{-/-}$ iBMDMs were primed with 100 ng/mL LPS for 6 h, exposed to peptides (5, 10, 20 μM) or DMSO (in largest peptide volume used) for 0.5 h before the addition of 1000 μg/mL flagellin/DOTAP for 4 h. Mean values and standard deviations of at least two repeats are shown. Results are representative of 2 independent experiments.

d – IL-1β levels by ELISA assay after iBMDMs were primed with 100 ng/mL LPS for 6 h, exposed to peptides (10, 20, 30, 40 μM) or DMSO (in largest peptide volume used) for 0.5 h before the addition of 1 μg/mL poly (dA:dT)/lipofectamin overnight. Mean values and standard deviations of at least two repeats are shown. Results are representative of 2 independent experiments.

Figure 5 ASC$^{PYD/H2-H3}$ binds NLRP3^{PYD} domain and crosses blood-brain barrier when equipped with Angiopep-2 tag

a – IL-1β levels by ELISA assay after immortalized microglia cells were primed with 100 ng/mL LPS for 6 h, exposed to peptides (10, 20, 30, 40 μM) or DMSO (in largest peptide volume used) for 0.5 h before the addition of 300 μg/mL aluminum salts overnight. Mean values and standard deviations of at least two repeats are shown. Results are representative of 2 independent experiments.

b – Sensorgrams showing the binding of Angiopep2-ASC$^{PYD/H2-H3}$ analyte at increasing concentrations injected onto the NTA chip-immobilized NLRP3^{PYD}-Histag ligand. The specific binding to the ligand was recorded in response units as the difference in signal between ligand-immobilized and empty flow cell upon analyte injection. Images are representative of 2 independent experiments.

c – Confocal microscopy images of immortalized microglia cells that underwent 0.5 h treatment with 20 μM Angiopep2-ASC$^{PYD/H2-H3}$-TMR (red) and had nuclei stained with DAPI (blue). Scale bar represents 50 μm. Images are representative of 2 independent experiments.

d – Confocal microscopy images of histological slides of organs collected from mice 1h after the i.v. injection of either 0.3 μmol/mouse Angiopep2-ASC$^{PYD/H2-H3}$-TMR or ASC$^{PYD/H2-H3}$-TMR. Images were converted to grayscale and adjustments made in brightness and contrast in ImageJ. Scale bar represents 250 μm.

Figure 6 Peptide ASC$^{PYD/H2-H3}$ effectively inhibited silica-induced peritonitis in mouse model

a – Schematic representation of the animal experiment.

b – Neutrophil count in the collected peritoneal lavage of treated mice (as shown above) as determined by flow cytometry using FITC labeled anti-mouse Ly-6G (Gr-1) antibody targeting Gr1 neutrophil marker. Mean and SEM is shown. For comparison of peptide-treated group with DMSO-treated group unpaired two-tailed t-test with Welch's correction was used.

Figure 1

a

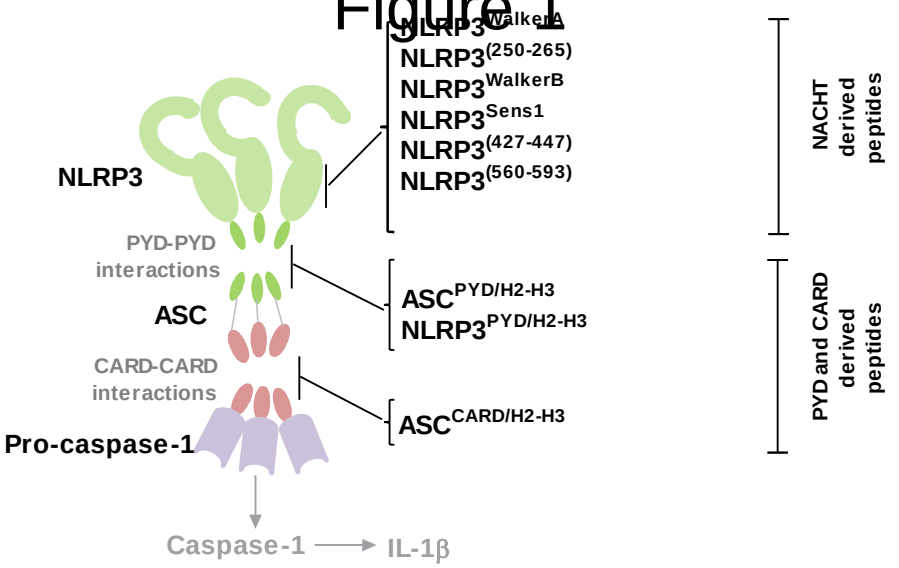
NLRP3
PYD-PYD interactions
ASC
CARD-CARD interactions
Pro-caspase-1
Caspase-1 → IL-1β
NLRP3WalkerA
NLRP3(250-265)
NLRP3WalkerB
NLRP3Sens1
NLRP3(427-447)
NLRP3(560-593)
NACHT derived peptides
ASCPYD/H2-H3
NLRP3PYD/H2-H3
ASCCARD/H2-H3
PYD and CARD derived peptides

b

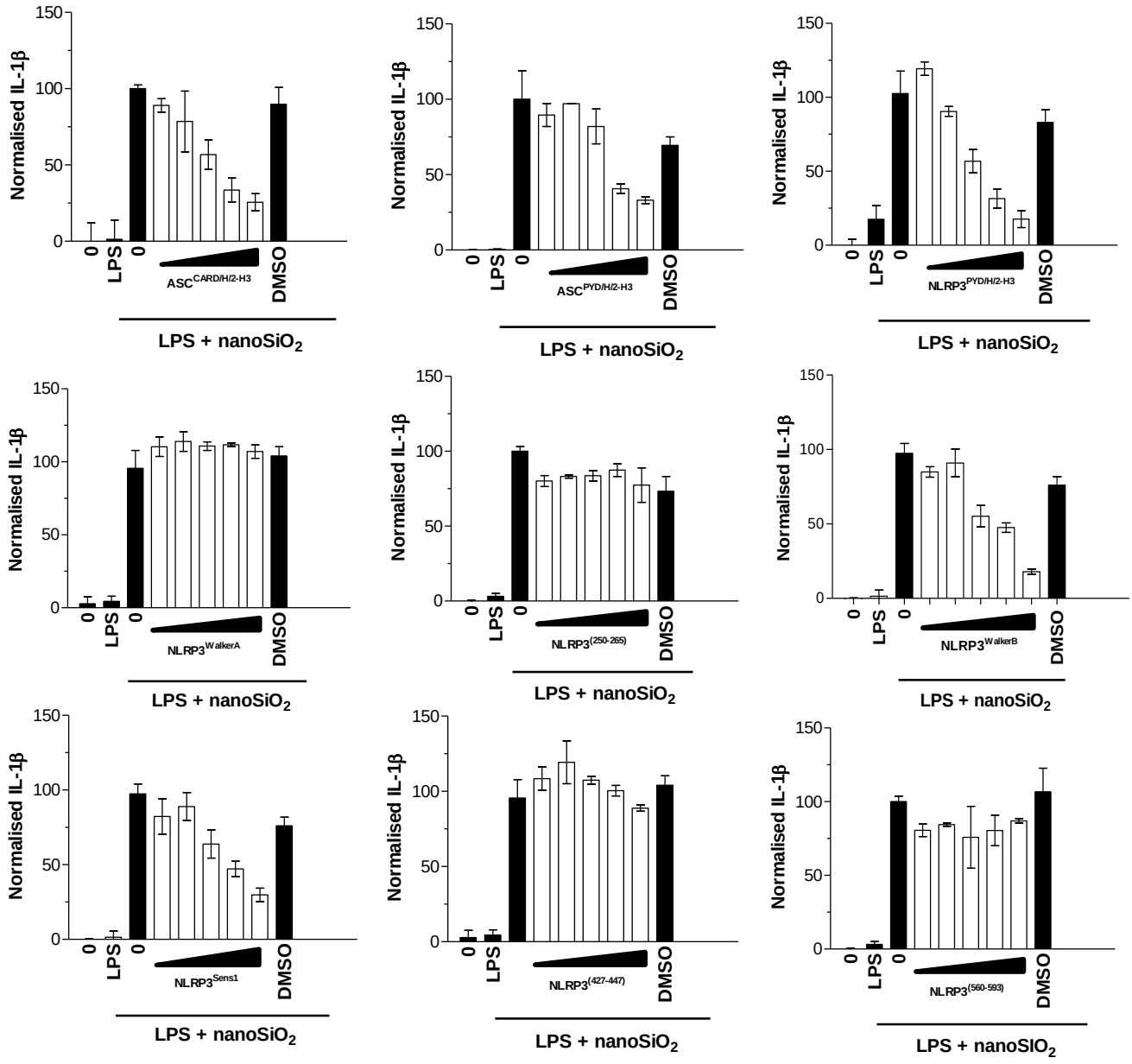
Normalised IL-1β
150
100
50
0
0
LPS
0
ASCCARD/H2-H3
DMSO
LPS + nanoSiO2
ASCPYD/H2-H3
NLRP3PYD/H2-H3
NLRP3WalkerA
NLRP3(250-265)
NLRP3WalkerB
NLRP3Sens1
NLRP3(427-447)
NLRP3(560-593)
LPS + nanoSIO2

Figure 2

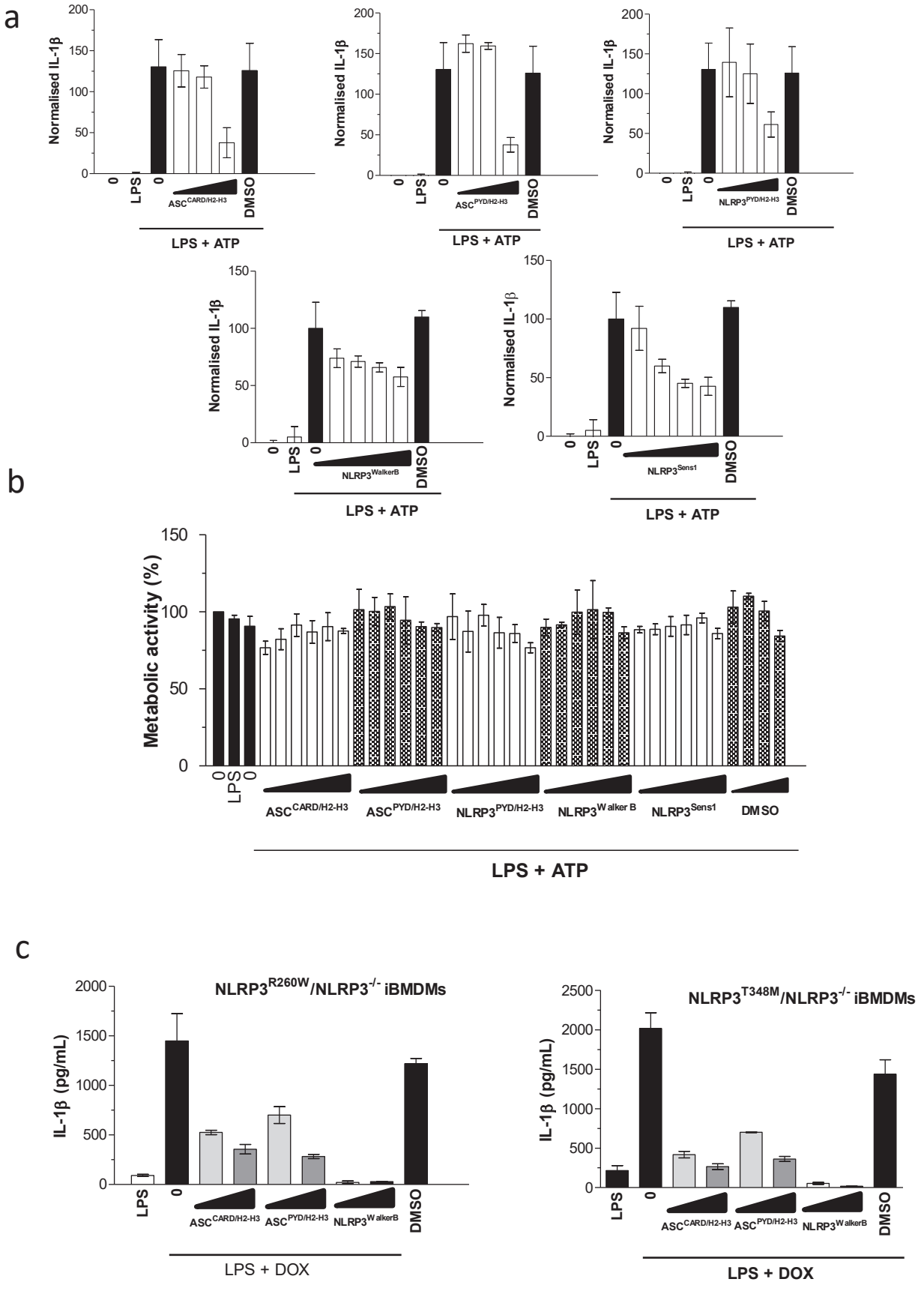
a
Normalised IL-1β
LPS
0
ASC^CARD/H2-H3
ASC^PYD/H2-H3
NLRP3^PYD/H2-H3
NLRP3^WalkerB
NLRP3^Sens1
DMSO
LPS + ATP
b
Metabolic activity (%)
ASC^CARD/H2-H3
ASC^PYD/H2-H3
NLRP3^PYD/H2-H3
NLRP3^W alker B
NLRP3^Sens1
DMSO
LPS + ATP
c
NLRP3^R260W/NLRP3^-/- iBMDMs
NLRP3^T348M/NLRP3^-/- iBMDMs
IL-1β (pg/mL)
LPS + DOX

Figure 3

a

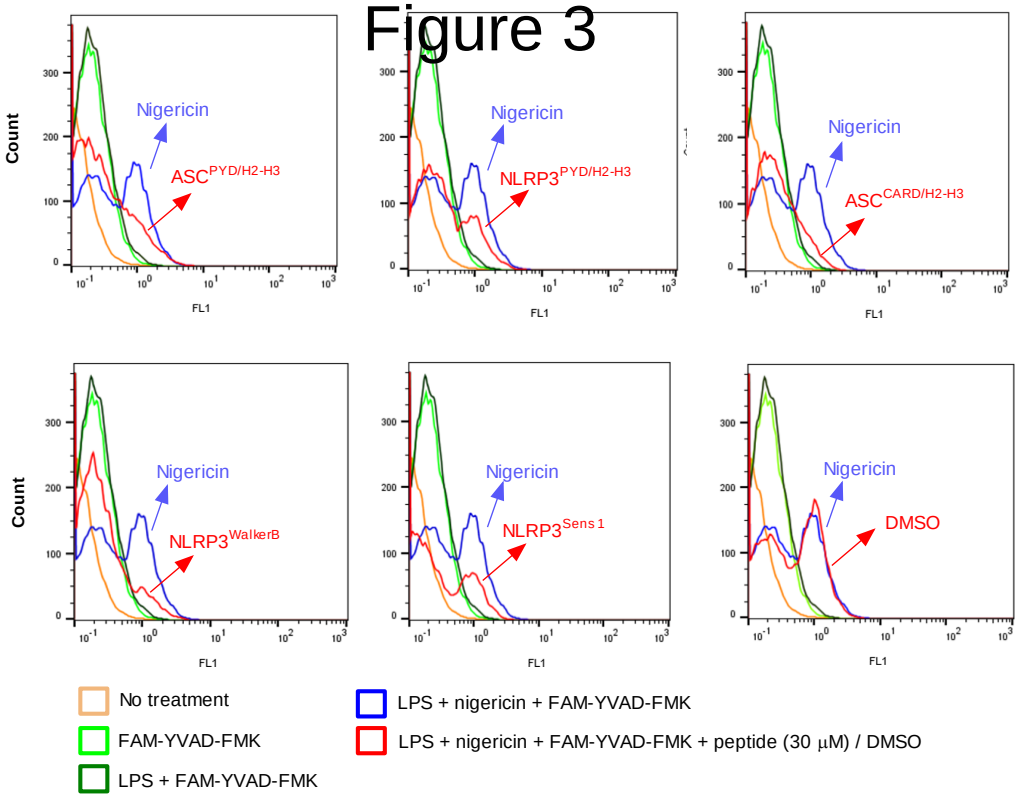
Count
Nigericin
ASC^PYD/H2-H3
NLRP3^PYD/H2-H3
ASC^CARD/H2-H3
NLRP3^WalkerB
NLRP3^Sens1
DMSO
FL1
No treatment
FAM-YVAD-FMK
LPS + FAM-YVAD-FMK
LPS + nigericin + FAM-YVAD-FMK
LPS + nigericin + FAM-YVAD-FMK + peptide (30 μM) / DMSO

b

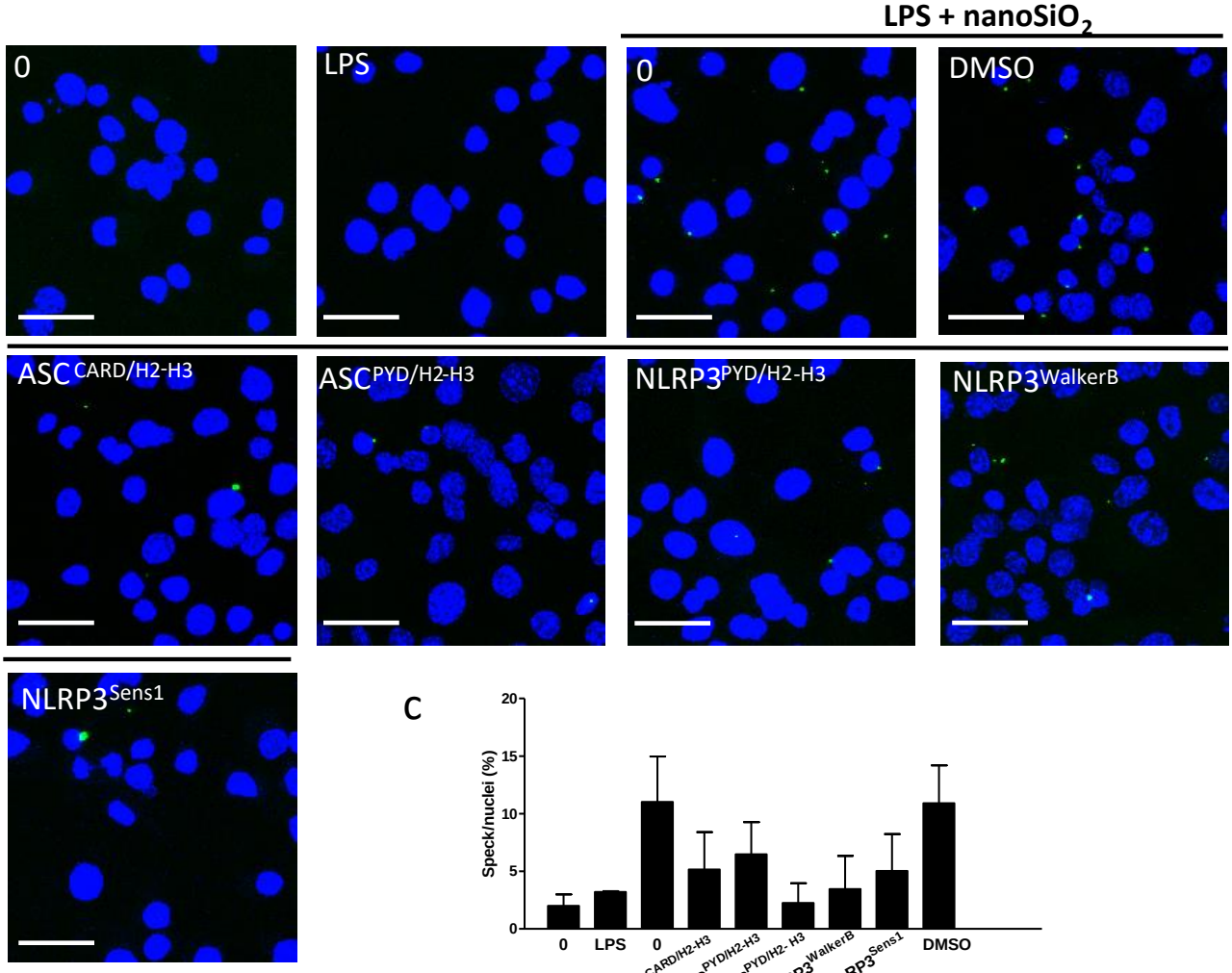
LPS + nanoSiO2
0
LPS
0
DMSO
ASC CARD/H2-H3
ASC PYD/H2-H3
NLRP3 PYD/H2-H3
NLRP3 WalkerB
NLRP3 Sens1

c

Speck/nuclei (%)
20
15
10
5
0
0
LPS
0
ASC CARD/H2-H3
ASC PYD/H2-H3
NLRP3 PYD/H2- H3
NLRP3 WalkerB
NLRP3 Sens1
DMSO
LPS + nanoSiO2

Figure 4

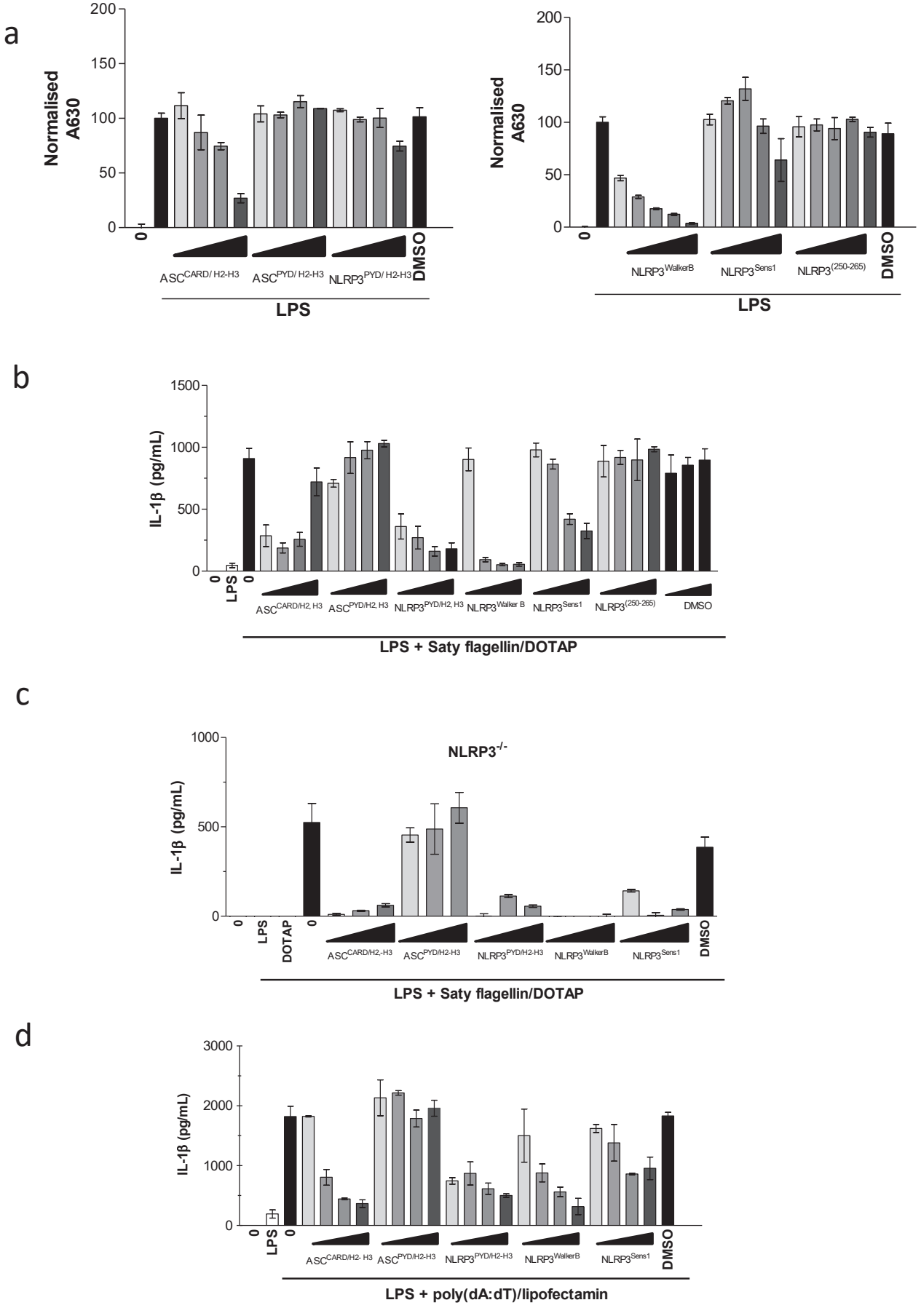
a
Normalised A630
200
150
100
50
0
0
ASC^CARD/ H2-H3
ASC^PYD/ H2-H3
NLRP3^PYD/ H2-H3
DMSO
LPS
NLRP3^WalkerB
NLRP3^Sens1
NLRP3^(250-265)
b
IL-1β (pg/mL)
1500
1000
500
LPS
ASC^CARD/H2, H3
ASC^PYD/H2, H3
NLRP3^PYD/H2, H3
NLRP3^Walker B
NLRP3^Sens1
NLRP3^(250-265)
DMSO
LPS + Saty flagellin/DOTAP
c
NLRP3^-/-
DOTAP
ASC^CARD/H2,-H3
ASC^PYD/H2-H3
NLRP3^PYD/H2-H3
NLRP3^WalkerB
NLRP3^Sens1
d
3000
2000
ASC^CARD/H2- H3
LPS + poly(dA:dT)/lipofectamin

Figure 5

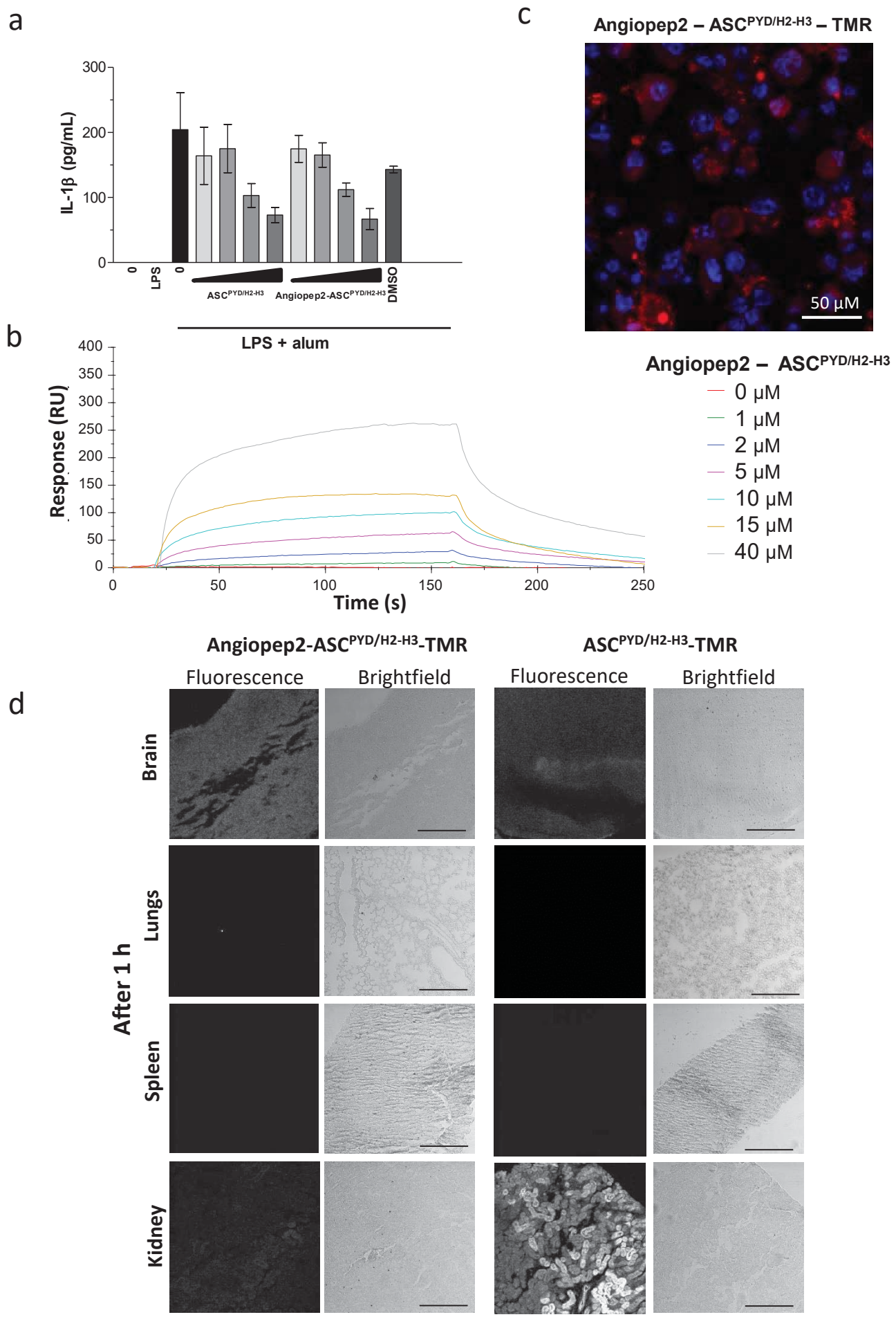
a
IL-1β (pg/mL)
300
200
100
0
0
LPS
0
ASC^PYD/H2-H3
Angiopep2-ASC^PYD/H2-H3
DMSO
b
LPS + alum
Response (RU)
400
350
300
250
200
150
100
50
0
0
50
100
150
200
250
Time (s)
Angiopep2 – ASC^PYD/H2-H3
0 µM
1 µM
2 µM
5 µM
10 µM
15 µM
40 µM
c
Angiopep2 – ASC^PYD/H2-H3 – TMR
50 µM
d
Angiopep2-ASC^PYD/H2-H3-TMR
ASC^PYD/H2-H3-TMR
Fluorescence
Brightfield
Fluorescence
Brightfield
After 1 h
Brain
Lungs
Spleen
Kidney

Figure 6

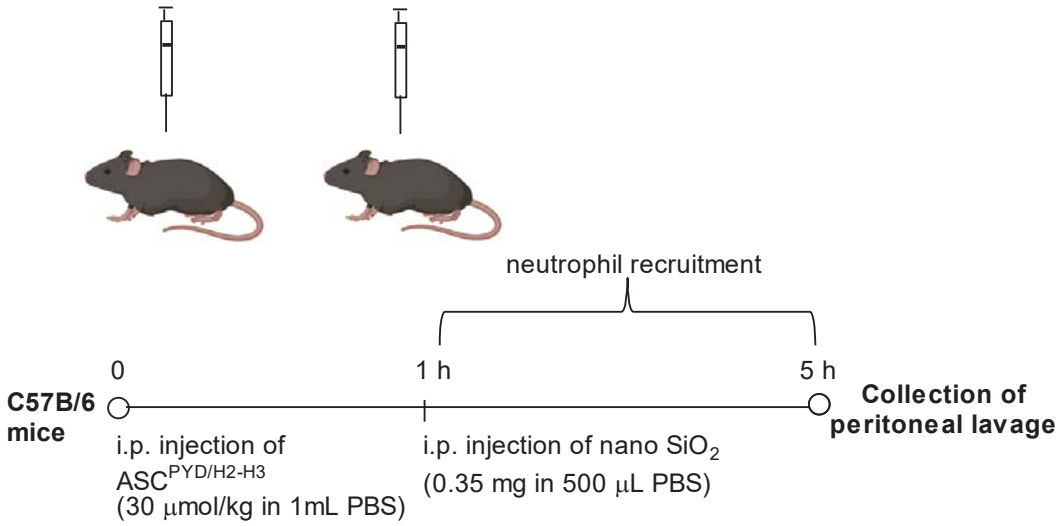
neutrophil recruitment
0
1 h
5 h
C57B/6 mice
Collection of peritoneal lavage
i.p. injection of ASC^PYD/H2-H3 (30 μmol/kg in 1mL PBS)
i.p. injection of nano SiO2 (0.35 mg in 500 μL PBS)

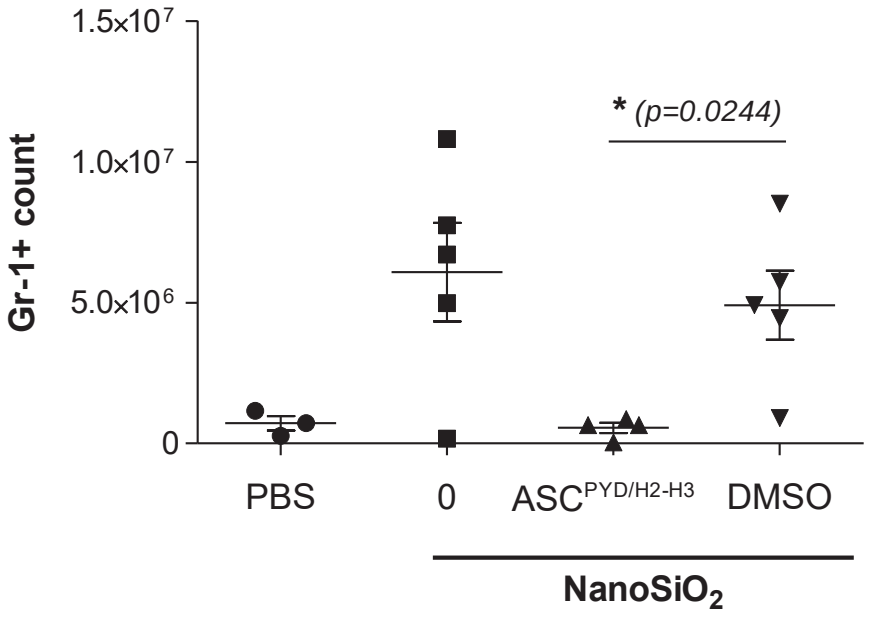
1.5x10^7
1.0x10^7
5.0x10^6
0
Gr-1+ count
* (p=0.0244)
PBS
0
ASC^PYD/H2-H3
DMSO
NanoSiO2

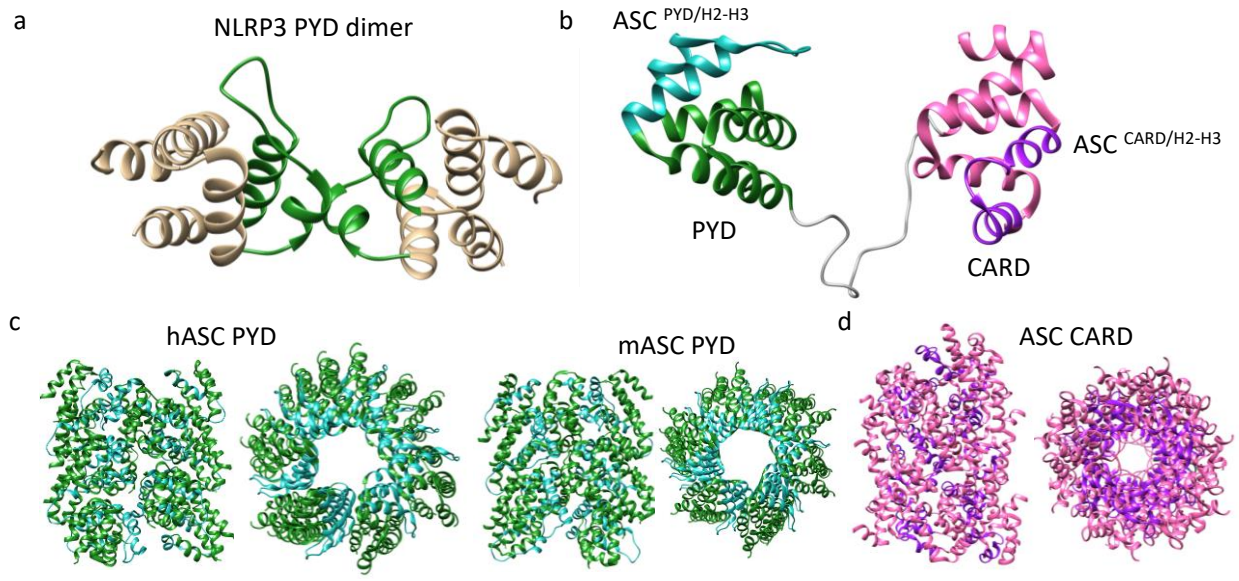

Figure S1 Structures of PYD and CARD domains with labeled selected peptide segments
a – NLRP3^{PYD} dimer (based on the structure PDB ID: 3QF2 (1)) with H2-H3 segment labeled in green.
b – ASC comprises PYD (green) and CARD (pink) domains (PBD ID: 2KN6 (2)). H2-H3 segments in PYD and CARD are labeled in cyan and violet, respectively.
c – ASC^{PYD} filament from human (PDB ID: 3J63 (3) and mouse (PDB ID: 2N1F (4)) with H2-H3 segment labeled in cyan.
d – ASC^{CARD} filament (PDB ID: 6N1H (5)).

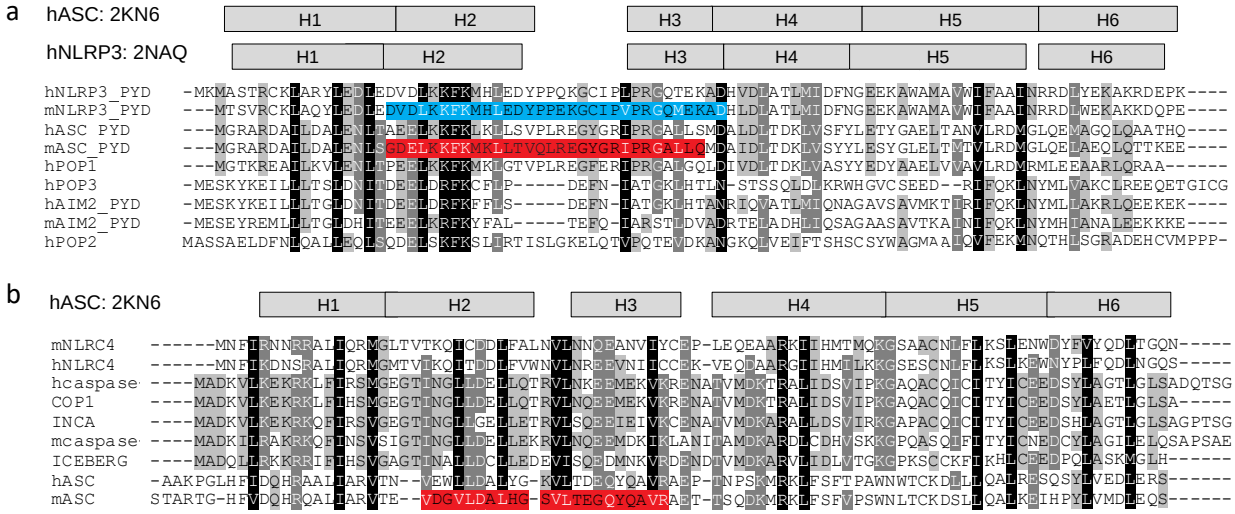

Figure S2 Sequence alignments of PYD and CARD domains
a – Sequence alignments of PYD domains from human and mouse NLRP3, ASC and AIM2 orthologues and pyrin-only proteins. Secondary structures based on structures of ASC (PBD ID: 2KN6 (2)) and NLRP3 (PBD ID: 2NAQ (6)) are depicted above alignment. Sequence corresponding to NLRP3$^{PYD/H2-H3}$ is highlighted in blue and the one corresponding to ASC$^{PYD/H2-H3}$ in red.
b – Sequence alignments of CARD domains from various inflammasome related proteins and their regulators. Secondary structure based on structure of ASC (PBD ID: 2KN6 (2)) is depicted above alignment. Sequence corresponding to ASC$^{CARD/H2-H3}$ is highlighted in red.

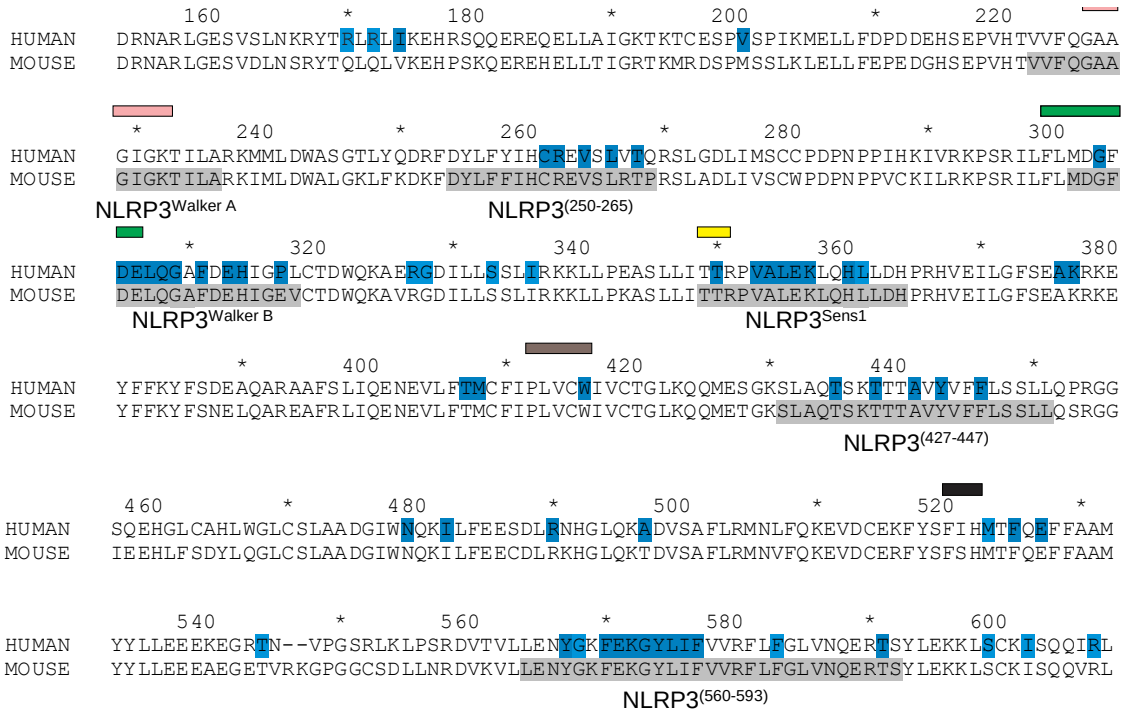

Figure S3 Alignment of mouse and human NLRP3^{NACHT} domain protein sequences
Amino acid residues which are mutated in CAPS are depicted in blue in human NLRP3 sequence. Selected peptide segments are highlighted in grey in mouse NLRP3 sequence. ATP binding motifs are labelled above sequences as follows: Walker A –pink, Walker B-green, Sensor 1-yellow, PhhCW motif- grey, WH-His- black.

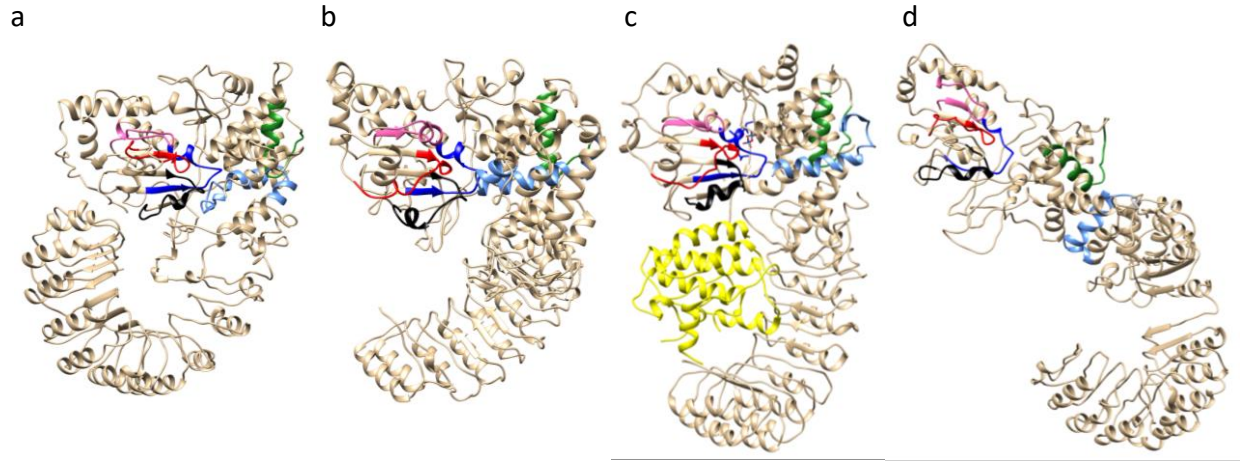

Figure S4 Peptide segments mapped on the homology models of mouse NLRP3
Models are based on the structures of NLRC4 (a,d) and NLRC2 (b), and corresponding segments mapped on the structure of human NLRP3-NEK7 complex (PDB ID: 6NPY (7)) (c) Models of mouse NLRP3 based on closed NLRC4 structure (8) (a), NLRC2 (9) (b) and open NLRC4 structure (10) were predicted with I-TASSER. NLRP3^{WalkerA} is coloured in blue, NLRP3$^{(250-265)}$ in pink, NLRP3^{WalkerB} in red, NLRP3^{Sens1} in black, NLRP3$^{(427-447)}$ in green and NLRP3$^{(560-593)}$ in light blue. NEK7 is coloured in yellow (in c).

Peptide	Aminoacid sequence (N to C terminus)	Modification
$ASC^{CARD/H2-H3}$	WGGVDGVLDALHGSVLTEGQYQAVRK	Myristoylation
$ASC^{PYD/H2-H3}$	WGGGDELKKFKMKLLTVQLREGYGRIPRGALLQK	Myristoylation
$NLRP3^{PYD/H2-H3}$	WGGDVDLKKFKMHLEDYPPEKGCIPVPRGQMEKADK	Myristoylation
$NLRP3^{Walker\ A}$	VVFQGAAGIGKTILA	Myristoylation
$NLRP3^{(250-265)}$	DYLFFIHCREVSLRTP	Myristoylation
$NLRP3^{WalkerB}$	MDGFDELQGAFDEHIGEV	Myristoylation
$NLRP3^{Sens1}$	TTRPVALEKLQHLLDH	Myristoylation
$NLRP3^{(427-447)}$	SLAQTSKTTTAVYVFFLSSLL	Myristoylation
$NLRP3^{(560-593)}$	LENYGKFEKGYLIFVVRFLFGLVNQERTSYLEKK	Myristoylation
Angiopep2-$ASC^{PYD/H2-H3}$-TMR	TFFYGGSRGKRNNFKTEEYGDELKKFKMKLLTVQLREGY GRIPRGALLQK	TMR
Antennapedia-$ASC^{PYD/H2-H3}$-TMR	RQIKIWFQNRRMKWKKGGGDELKKFKMKLLTVQLREGYG RIPRGALLQK	TMR
$ASC^{PYD/H2-H3}$-TMR	GDELKKFKMKLLTVQLREGYGRIPRGALLQK	TMR
Angiopep2-$ASC^{PYD/H2-H3}$	TFFYGGSRGKRNNFKTEEYGDELKKFKMKLLTVQLREGY GRIPRGALLQK	/
Scrambled $ASC^{PYD/H2-H3}$	WGGLRGKLGLYKQDFRIQGMEKARLELGTVKPLK	Myristoylation

Figure S5 An overview of peptide modulators and their biochemical properties
GenScript online tool Peptide Molecular Weight Calculator was used to analyse biochemical properties **(**red - acidic residue, blue – basic residue, green - hydrophobic residue).

REFERENCES

1. Bae, J. Y. and Park, H. H. (2011) Crystal Structure of NALP3 Protein Pyrin Domain (PYD) and Its Implications in Inflammasome Assembly. *J. Biol. Chem.* **286**, 39528–39536

2. de Alba, E. (2009) Structure and Interdomain Dynamics of Apoptosis-associated Speck-like Protein Containing a CARD (ASC). *J. Biol. Chem.* **284**, 32932–32941

3. Lu, A., Magupalli, V. G., Ruan, J., Yin, Q., Atianand, M. K., Vos, M. R., Schr??der, G. F., Fitzgerald, K. A., Wu, H., and Egelman, E. H. (2014) Unified polymerization mechanism for the assembly of asc-dependent inflammasomes. *Cell* **156**, 1193–1206

4. Sborgi, L., Ravotti, F., Dandey, V. P., Dick, M. S., Mazur, A., Reckel, S., Chami, M., Scherer, S., Huber, M., Böckmann, A., Egelman, E. H., Stahlberg, H., Broz, P., Meier, B. H., and Hiller, S. (2015) Structure and assembly of the mouse ASC inflammasome by combined NMR spectroscopy and cryo-electron microscopy. *Proc. Natl. Acad. Sci. U. S. A.* **112**, 13237–13242

5. Li, Y., Fu, T. M., Lu, A., Witt, K., Ruan, J., Shen, C., and Wu, H. (2018) Cryo-EM structures of ASC and NLRC4 CARD filaments reveal a unified mechanism of nucleation and activation of caspase-1. *Proc. Natl. Acad. Sci. U. S. A.* **115**, 10845–10852

6. Oroz, J., Barrera-Vilarmau, S., Alfonso, C., Rivas, G., and De Alba, E. (2016) ASC pyrin domain self-associates and binds NLRP3 protein using equivalent binding interfaces∗. *J. Biol. Chem.* **291**, 19487–19501

7. Sharif, H., Wang, L., Wang, W. L., Magupalli, V. G., Andreeva, L., Qiao, Q., Hauenstein, A. V., Wu, Z., Núñez, G., Mao, Y., and Wu, H. (2019) Structural mechanism for NEK7-licensed activation of NLRP3 inflammasome. *Nature* **570**, 338–343

8. Hu, Z., Yan, C., Liu, P., Huang, Z., Ma, R., Zhang, C., Wang, R., Zhang, Y., Martinon, F., Miao, D., Deng, H., Wang, J., Chang, J., and Chai, J. (2013) Crystal structure of NLRC4 reveals its autoinhibition mechanism. *Science* **341**, 172–175

9. Maekawa, S., Ohto, U., Shibata, T., Miyake, K., and Shimizu, T. (2016) Crystal structure of NOD2 and its implications in human disease. *Nat. Commun.* **7**

10. Zhang, L., Chen, S., Ruan, J., Wu, J., Tong, A. B., Yin, Q., Li, Y., David, L., Lu, A., Wang, W. L., Marks, C., Ouyang, Q., Zhang, X., Mao, Y., and Wu, H. (2015) Cryo-EM structure of the activated NAIP2-NLRC4 inflammasome reveals nucleated polymerization. *Science (80-.).* **350**, 404–409

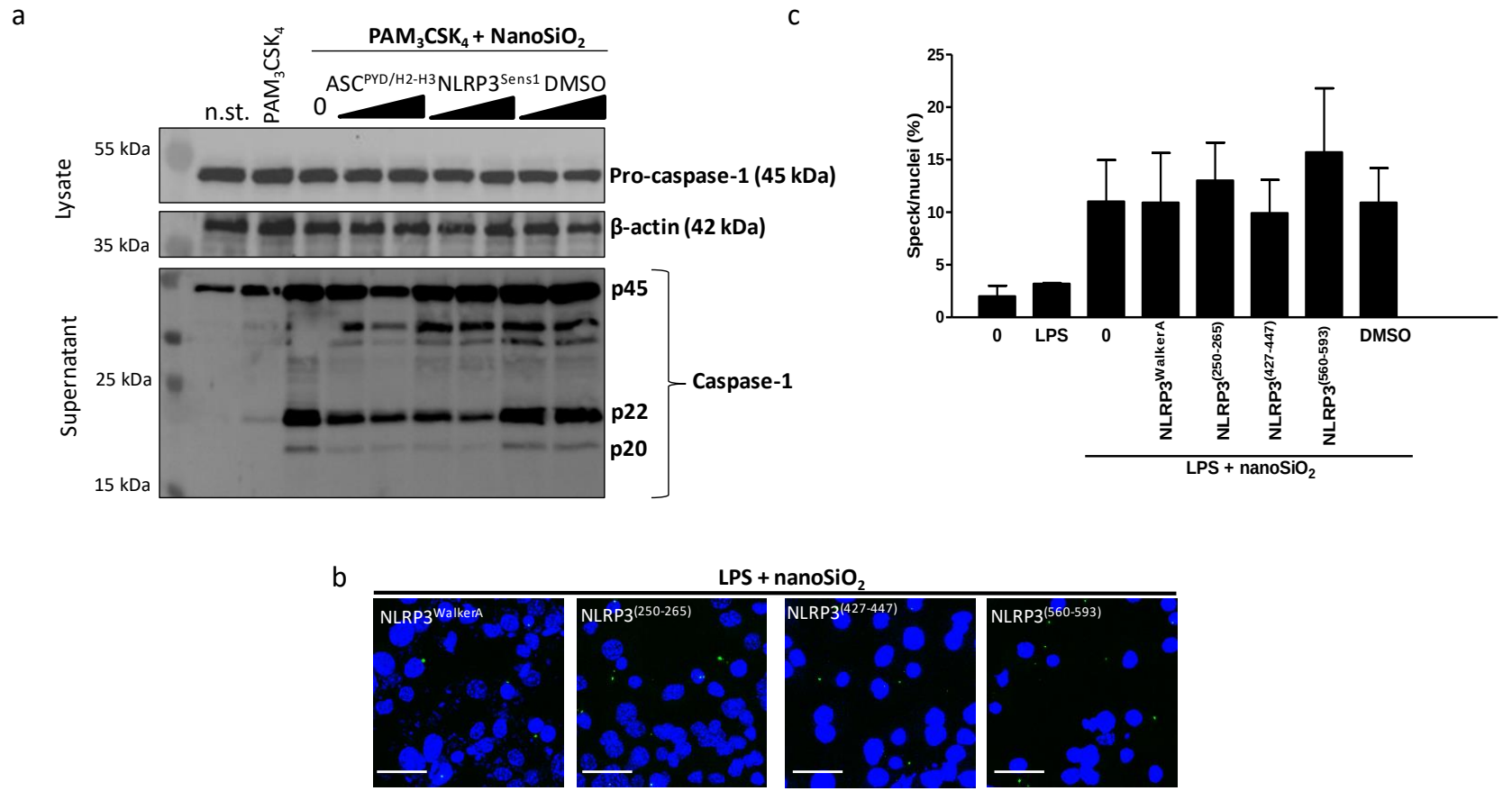

Figure S6 Peptides not affecting IL-1β do not affect ASC oligomerisation

a – Caspase-1 detection by Western blotting after iBMDMs were primed with 500 ng/mL PAM_3CSK_4 overnight and treated with 20 and 40 μM peptides or DMSO in equivalent concentrations for 0.5 h before stimulation with 190 ng/mL $nanoSiO_2$ for 4h. Cells lysates and supernatants were collected and analysed for pro-caspase-1 and caspase-1 levels, respectively. Results are representative of 2 independently repeated experiments. b, c – ASC speck detection after iBMDMs were primed with 100 ng/mL LPS for 6h and exposed to 40 μM peptides or DMSO (concentration equivalent to the one present at highest peptide concentration) for 0.5h before the addition of 190 ng/mL $nanoSiO_2$ for 4h. Cells were subsequently fixed, permeabilized and labelling of ASC specks (AlexaFluor488, green) and nuclei (DAPI, blue) was performed. The images are a part of experiment presented in figure 3b,c. Representative images (b) and mean speck/nuclei ratio and standard deviations based on at least 6 confocal microscopy images (c) are shown. Adjustments were made in brightness and contrast in LAS X and images cropped in ImageJ. Results are a representative of 2 independently repeated experiments. Scale bar = 30 μm.

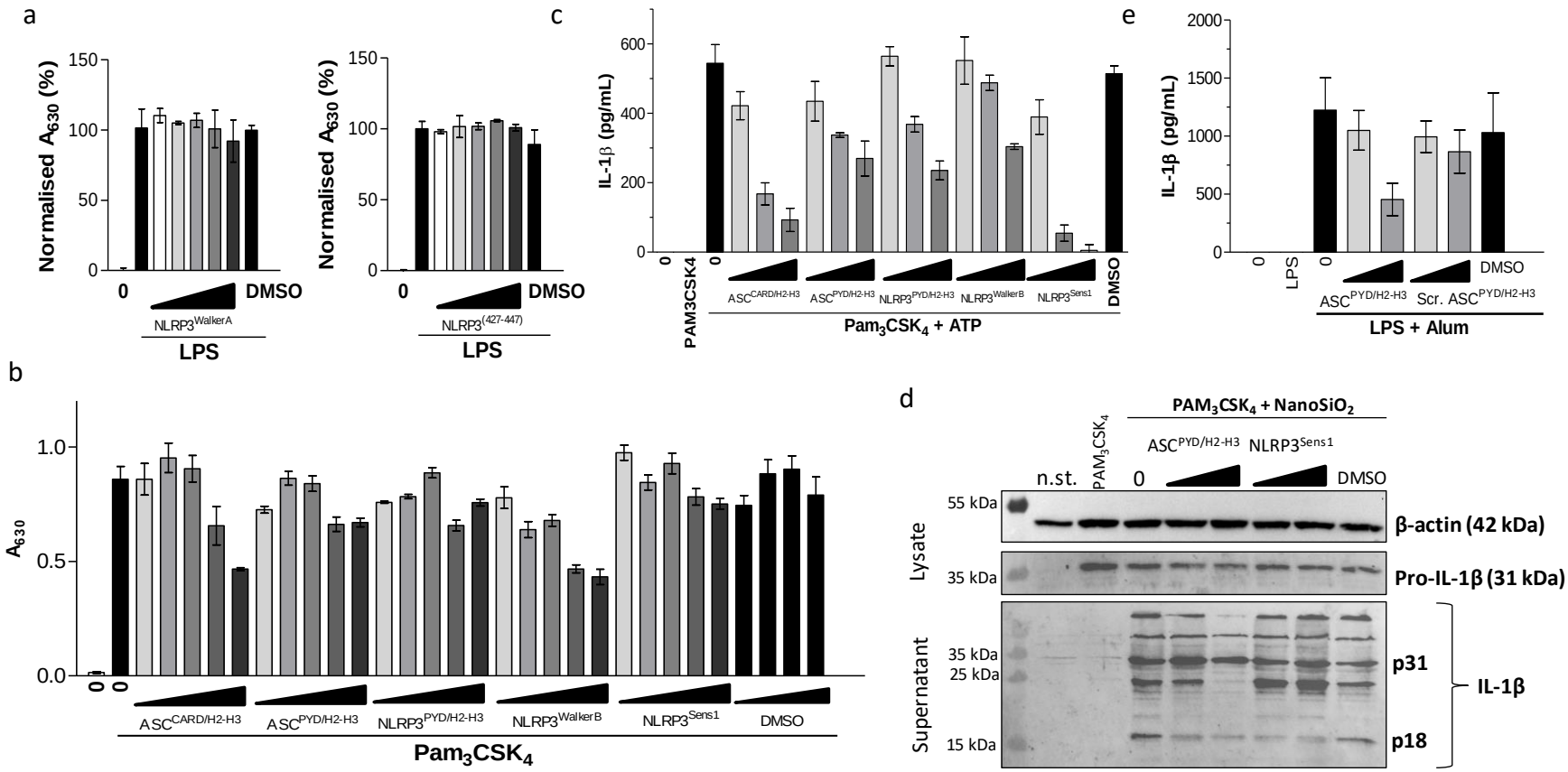

Figure S7 Effect of inhibitory peptides on the priming and sequence specific inhibition by ASC$^{PYD/H2-H3}$
a – SEAP levels with QUANTI-Blue assay after RAWBlue cells were exposed to peptides (1, 5, 10, 20, 40 μM) or DMSO (corresponding to concentration at the highest peptide concentration used) for 0.5 h before overnight priming with 50ng/mL LPS. Average absorbance at 630 nm and standard deviations of at least two repeats are shown. Results are representative of 2 independent experiments. b – SEAP levels with QUANTI-Blue assay after RAWBlue cells were exposed to peptides (1, 5, 10, 20, 40 μM) or DMSO for 0.5 h before 16 h priming with 100ng/mL PAM_3CSK_4. Average absorbance at 630 nm and standard deviations of at least two repeats are shown. Results are representative of 2 independent experiments. c – IL-1β levels with ELISA assay after iBMDMs were primed with 1 μg/mL PAM_3CSK_4 for 6 h and exposed to peptides (5, 20, 40 μM) for 0.5 h before the addition of 5 mM ATP for 1 h. Mean values and standard deviations of at least two repeats are shown. Results are representative of 2 independent experiments. d – IL-1β detection by Western blotting after iBMDMs were primed with PAM_3CSK_4 (200 ng/mL, overnight). After medium replacement cells were treated with 20 and 40 μM inhibitory peptides ASC$^{PYD/H2-H3}$ and NLRP3^{Sens1} or DMSO. Cells were then stimulated with $nanoSiO_2$ for 3h. Cell lysates were analysed for pro-IL-1β while mature IL-1β levels were assessed in the concentrated supernatants. Results are representative of 2 independently repeated experiments. e – IL-1β levels with ELISA assay after iBMDMs were primed with 100 ng/mL LPS for 6h, exposed to ASC$^{PYD/H2-H3}$ peptide, its scrambled version (both 20, 40 μM) or DMSO for 0.5 h before the addition of alum 300 μg/mL for overnight incubation. Mean values and standard deviations of at least two repeats are shown. Results are representative of 2 independent experiments.

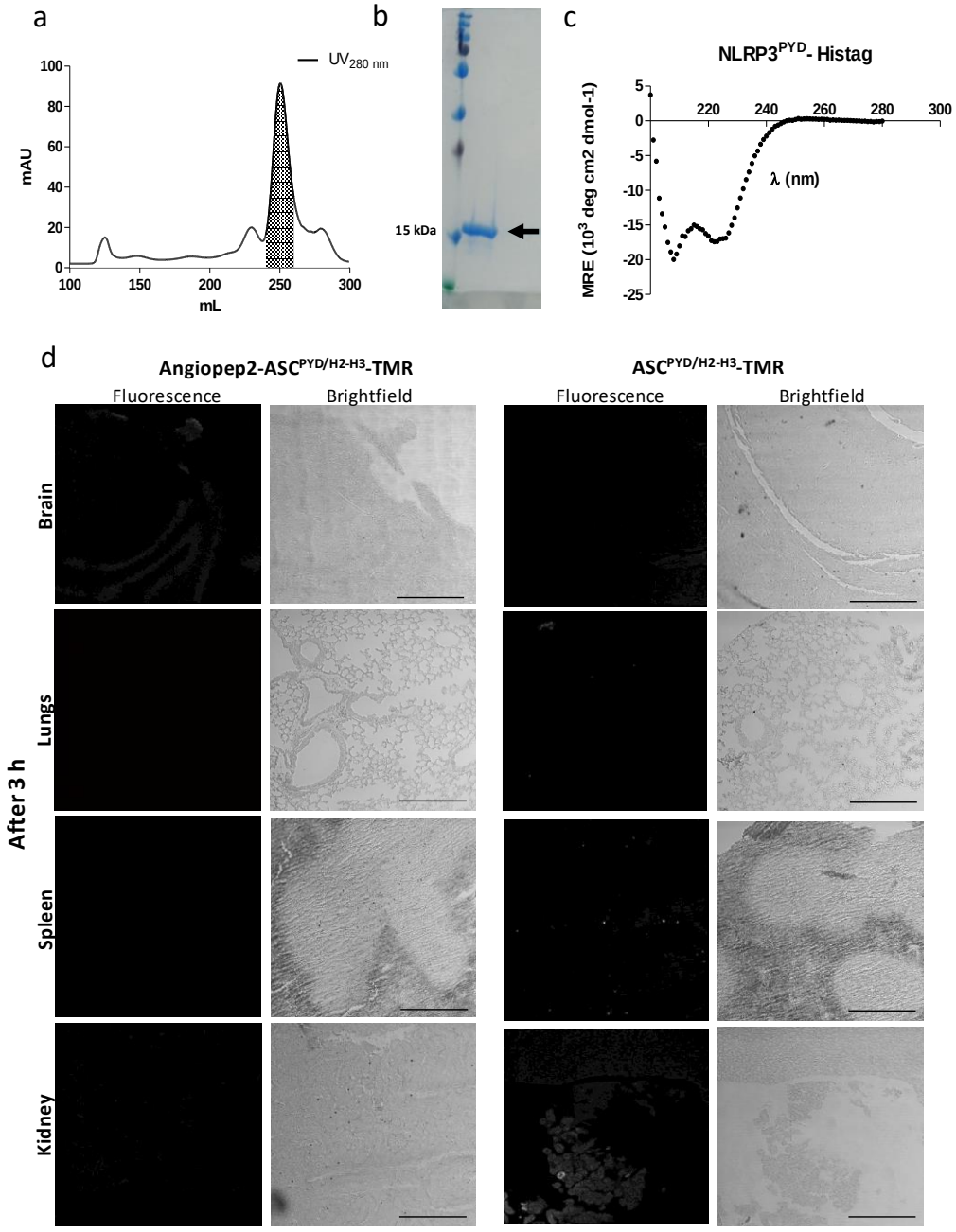

Figure S8 ASC$^{PYD/H2-H3}$ binds NLRP3^{PYD} domain and crosses blood-brain barrier when equipped with Angiopep-2 tag

a – SEC chromatogram of NLRP3^{PYD}-Histag construct isolated from NiCo2 (DE3) production strain after IPTG induction. Monomer (shaded) was used for further experiments.

b – SDS Page electrophoresis of NLRP3^{PYD}-Histag construct

c – CD spectrum of monomeric NLRP3^{PYD}-Histag

d – Confocal microscopy images of histological slices of organs collected from mice 3h after the i.v. injection of either 0.3 μmol/mouse Angiopep2-ASC$^{PYD/H2-H3}$-TMR or ASC$^{PYD/H2-H3}$-TMR. Images were converted to grayscale and adjustments made in brightness and contrast in ImageJ. Scale bar = 250 μm.

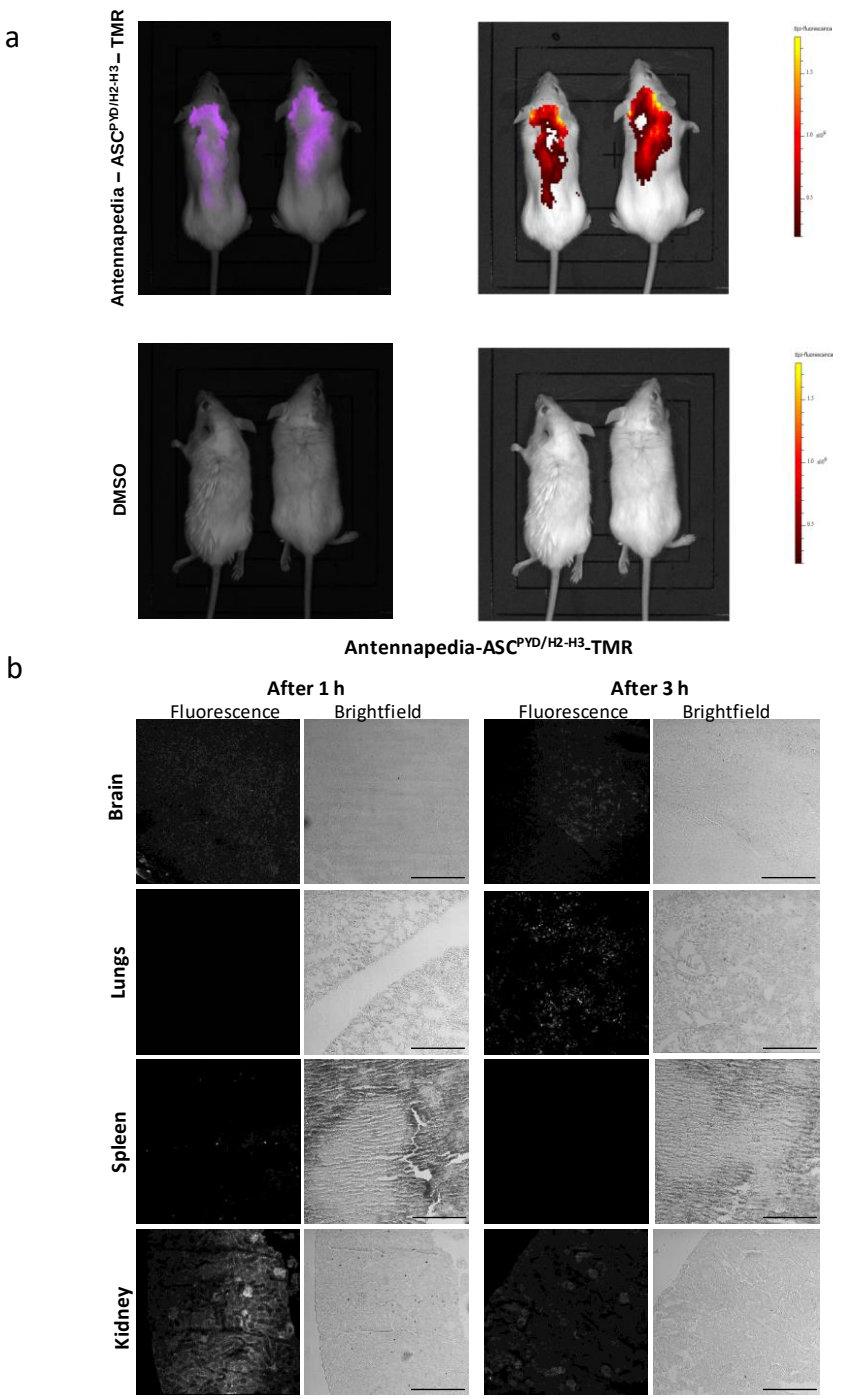

Figure S9 ASC$^{PYD/H2-H3}$ crosses blood-brain barrier when equipped with Antennapedia tag
a – *In vivo* fluorescence imaging of sacrificed mice after the i.v. injection of Antennapedia-ASC$^{PYD/H2-H3}$-TMR or DMSO with (right) and without (left) spectral unmixing. Colour scale shows radiant efficiency (p/sec/cm^2/sr)/(μW/cm^2).
b – Confocal microscopy images of histological slices of organs collected from mice 1h or 3h after the i.v. injection of 0.3 μmol/mouse Antennapedia-ASC$^{PYD/H2-H3}$-TMR. Fluorescence images (left) were converted to grayscale and adjustments made in brightness and contrast in ImageJ. Scale bar = 250 μm.